

1 Main Manuscript for

2 **Hygroscopicity of Isoprene-Derived Secondary Organic Aerosol Mixture Proxies:**
3 **Importance of Diffusion and Salting In Effects**

4 Nahin Ferdousi-Rokib^{1*}, N. Cazimir Armstrong², Stephanie Jacoby³, Alana J. Doder⁴, Martin
5 Ahn¹, Ergine R. Remy¹, Zhenfa Zhang², Avram Gold², Joseph L. Woo⁵, Yue Zhang⁴, Jason D.
6 Surratt^{2,6}, Akua A. Asa-Awuku^{1,3}

7 ¹Department of Chemical and Biomolecular Engineering, University of Maryland, College Park,
8 MD 20742, United States

9 ²Department of Environmental Sciences and Engineering, University of North Carolina at
10 Chapel Hill, Chapel Hill, North Carolina 27599, United States

11 ³Department of Chemistry and Biochemistry, University of Maryland, College Park, MD 20742,
12 United States

13 ⁴Department of Atmospheric Sciences, Texas A&M University, College Station, Texas 77843,
14 United States

15 ⁵Department of Chemical and Biomolecular Engineering, Lafayette College, Easton, PA 18042,
16 United States

17 ⁶Department of Chemistry, University of North Carolina at Chapel Hill, Chapel Hill, North
18 Carolina 27599, United States

19 *Now at: Department of Environmental Health and Engineering, Whiting School of Engineering,
20 Johns Hopkins University, Baltimore, MD 21218, United States

21 Keywords: Hygroscopicity, Organic Aerosols, IEPOX, SOA, viscosity, AFM

22 Correspondence to: Nahin Ferdousi-Rokib (ferdousn19@gmail.com) and Akua A. Asa-Awuku
23 (asaawuku@umd.edu)

24

25

26

27

28

29

30

31

32

33 **Abstract**

34 Isoprene-derived secondary organic aerosol (SOA) constituents, such as the 2-methyltetrols (2-
35 MT) and 2-methyltetrol sulfates (2-MTS), have been readily detected in atmospheric aerosols
36 ($PM_{2.5}$) and within mixtures containing ammonium sulfate (AS). Despite its prevalence, the water
37 uptake of 2-MT, 2-MTS, and their mixtures are not well understood. In this study, we determine
38 the physicochemical properties (e.g., surface activity, diffusivity, phase morphology) of
39 synthesized 2-MT, 2-MTS samples, and their mixtures with AS. 2-MT and 2-MTS have been
40 identified as surface-active and viscous. Thus, dynamic surface tension ($\sigma_{s/a}$) measurements were
41 taken to determine organic diffusion coefficients (D_s). The droplet growth of organic/AS mixtures
42 was measured under subsaturated conditions using a humidified tandem differential mobility
43 analyzer (H-TDMA) at $88.2\% RH \pm 1.5\%$. Droplet activation was measured under supersaturated
44 ($> 100\% RH$) conditions using a cloud condensation nuclei counter (CCNC); supersaturation (SS)
45 ranged from 0.3-1.4%. Hygroscopicity in both regimes were parameterized by the single
46 hygroscopicity parameter κ .

47 This study demonstrates how diffusion and salting-in effects influence the water uptake of
48 synthesized, isoprene-derived SOA mixtures. Results show that when mixed with AS, organic
49 diffusion for 2-MTS/AS becomes an order of magnitude faster while 2-MT diffusivity remains
50 unchanged. Both 2-MT/AS and 2-MTS aerosols present a plateau in subsaturated κ -values close
51 to pure AS. However, under supersaturated conditions, 2-MTS/AS behaves ideally, well-mixed ,
52 and can be characterized by κ -Köhler theory. Isoprene-derived SOA like 2-MT and 2-MTS
53 samples are ubiquitous, and thus, the impact from biogenic sources and its non-ideal
54 thermodynamic properties must be considered in aerosol-cloud interactions.

55
56
57
58
59
60
61
62
63
64
65
66
67

68 1. Introduction

69 Fine aerosol particles (PM_{2.5}) suspended within our atmosphere are a major contributor to Earth's
70 radiative forcing and uncertainties in global temperature projections (Intergovernmental Panel on
71 Climate, 2023). Aerosol-cloud radiative forcing uncertainty is attributed to aerosols' ability to
72 form and modify cloud properties, known as aerosol-cloud interactions or the "aerosol indirect
73 effect" (Köhler, 1936; Twomey, 1959; Twomey, 1974; Albrecht, 1989; Intergovernmental Panel
74 on Climate, 2023). An aerosol's ability to alter droplet formation is dependent on its
75 hygroscopicity or water uptake behavior under supersaturated conditions ($RH > 100\%$). In the
76 presence of water vapor, aerosols present a surface for condensation; droplet activation depends
77 on aerosol particle chemical composition and size (Seinfeld & Pandis, 1998; Petters &
78 Kreidenweis, 2007). The aerosol droplets can reach a point of unstable and uncontrollable growth,
79 thereby acting as cloud condensation nuclei (CCN) (Köhler, 1936; Seinfeld & Pandis, 1998).

80 Droplet models can apply Köhler theory to estimate aerosol droplet growth and CCN activity
81 (Köhler, 1936). In traditional Köhler theory, it is assumed that all aerosol solutes instantaneously
82 dissolve and contribute to water uptake (Petters & Kreidenweis, 2007). Aerosol hygroscopicity is
83 thus parameterized by Köhler theory through the single hygroscopicity parameter κ ; κ of mixed
84 composition is often estimated by the Zdanovskii-Stokes-Robinson (ZSR) mixing rule and it is
85 assumed that an individual solute's contribution to hygroscopicity is scaled by its volume fraction
86 (Petters & Kreidenweis, 2007). Thus, knowing aerosol composition is critical for understanding
87 CCN formation. However, κ -Köhler predictions of aerosol CCN activity neglect solute
88 physicochemical properties that may alter droplet growth. Previous studies have shown that
89 droplet-altering properties may be present within aerosols, such as the presence of complex
90 morphologies (e.g., inner core-outer layer), surface-activity, or salting in/salting out effects; as a
91 result, discrepancies between experimentally-determined κ and κ -Köhler predictions may occur
92 (Asa-Awuku & Nenes, 2007; Bertram et al., 2011; Song et al., 2013; Prisle & Mølgaard, 2018;
93 Riemer et al., 2019; Ott et al., 2020; Malek et al., 2023).

94 Field studies have observed the presence of internally mixed aerosols containing both inorganic
95 and organic compounds (Saxena, 1995; Murphy et al., 1998; Pratt & Prather, 2010). Inorganic
96 aerosols, primarily composed of salts like ammonium sulfate (AS) and sodium chloride have well-
97 defined hygroscopic properties. The ionic behavior of inorganic compounds promotes
98 instantaneous dissolution in water and contributes to CCN activation (Cziczo et al., 1997; Seinfeld,
99 2003; Rose et al., 2008; Laskina et al., 2015). However, fine organic aerosols (OA) pose a greater
100 challenge to aerosol hygroscopicity predictions. OA constitute 20-50% of atmospheric fine aerosol
101 mass and are diverse in composition. OA can be directly emitted into the atmosphere, referred to
102 as primary organic aerosols (POA) (Kanakidou et al., 2005). POA can originate from
103 anthropogenic (e.g., biomass burning and coal combustion) and biogenic (e.g., pollen) sources
104 (Seinfeld & Pandis, 1998; Kanakidou et al., 2005). In addition to POA, secondary organic aerosol
105 (SOA) can be formed through multigeneration gas-phase oxidation reactions of volatile organic
106 compounds (VOCs) or multiphase reactions of semi-/low-volatility organic compounds
107 (SVOCs/LVOCs) (Kanakidou et al., 2005). SOA is ubiquitous in the atmosphere, forming a major
108 component of fine OA mass (Zhang et al., 2007; Srivastava et al., 2022). For example, a study by

109 Zhang et al. (2007) found that SOA contributed 65% to 95% of OA mass in urban and remote
110 regions. Furthermore, SOA have been readily detected in mixtures with inorganic components,
111 such as AS (Yang et al., 2009; Zhu et al., 2017); indeed, a study by Zhu et al. (2017) estimated
112 66% of SOA as being internally mixed with sulfate. Thus, in addition to understanding pure
113 organic compounds, it is important to also study organic-inorganic interactions.

114 Previous studies have determined that a significant contributor to SOA is the aqueous-phase
115 chemical processing of isoprene-derived oxidation products (Claeys et al., 2004; Kanakidou et al.,
116 2005). Isoprene is a VOC emitted from biogenic sources and is considered one of the most
117 abundant biogenic VOCs (BVOCs). Isoprene emissions have been estimated to be ~ 500 Tg C
118 year⁻¹, rivaling methane emissions (Guenther et al., 2012; Sindelarova et al., 2014). Under alkyl
119 peroxy radical (RO₂·) + hydroperoxy radical (HO₂·) dominant conditions, isoprene is
120 photochemically oxidized by gas-phase hydroxyl radicals (·OH) to form large quantities of
121 isoprene-derived epoxydiols (IEPOX) (Paulot et al., 2009). IEPOX is then able to partition into
122 acidic sulfate-containing aerosol particles to produce isoprene-derived SOA (Surratt et al., 2010;
123 Lin et al., 2012; Gaston et al., 2014; Riva et al., 2019), which consists largely of 2-methyltetrols
124 (2-MT) and 2-methyltetrol sulfates (2-MTS).

125 Both 2-MT and 2-MTS were previously detected in atmospheric PM_{2.5}. For example, a study by
126 Claeys et al. (2004) found that 2-MT contributed 2% of organic carbon detected in PM_{2.5} collected
127 from the Amazon rainforest. Additional field studies have also found that 2-MTS can contribute
128 0.3-16.5% of total organic carbon in both the Amazon rainforest and Southeast US (Chan et al.,
129 2010; Froyd et al., 2010; Hettiyadura et al., 2019; Riva et al., 2019; Chen et al., 2021; Hughes et
130 al., 2021). The formation of both compounds can also alter aerosol particle composition and phase
131 state (Zhang et al., 2019a; Zhang et al., 2019b). For example, 2-MT and 2-MTS have been
132 observed to be in a semisolid or glassy state in aerosol particles (Chen et al., 2023). Highly viscous
133 SOA can exist in a glassy state; SOA viscosities can range from 10² to 10¹² Pa·s for ultraviscous
134 liquids or >10¹² Pa·s for amorphous, extremely viscous compounds (Virtanen et al., 2010;
135 Renbaum-Wolff et al., 2013; Zhang et al., 2015). Viscosity can influence organic solute dissolution
136 in droplets by slowing diffusion through the aqueous phase (Renbaum-Wolff et al., 2013). As a
137 result, slower organic diffusion rates can influence gas partitioning, particle shape, chemical aging,
138 multiphase reactions, and aerosol droplet growth (Riipinen et al., 2011; Shiraiwa & Seinfeld, 2012;
139 Zhang et al., 2015). Furthermore, studies incorporating SOA viscosity and phase state into larger,
140 global-scale models have observed changes to CCN and ice nuclei (IN) formation predictions
141 (Riipinen et al., 2011; Shiraiwa et al., 2017; Wolf et al., 2021). Thus, probing the viscosity and
142 resulting diffusion limitations may be necessary for understanding 2-MT and 2-MTS water uptake
143 properties (Chen et al., 2023).

144 Similar to other complex organic mixtures, the water uptake ability of isoprene-derived SOA can
145 be further complicated when mixed with inorganic components, such as AS. Previous studies have
146 observed the presence of internally-mixed SOA/AS aerosols in both the southeast US and Amazon;
147 in both regions a strong presence of 2-MT and 2-MTS has been observed (Chan et al., 2010; Froyd
148 et al., 2010; Bondy et al., 2018; Riva et al., 2019; Wu et al., 2019). The presence of inorganic salts
149 in aerosol mixtures can influence phase state based on organic physicochemical properties

150 (Topping, 2010; Ruehl et al., 2012; Ruehl et al., 2016; Malek et al., 2023). Inorganic compounds
151 can result in water solubility-limited and/or surface-active organics partitioning to a separated
152 phase (Ruehl et al., 2012; Ruehl et al., 2016; Freedman, 2017; Kang et al., 2020). As a result, the
153 partitioned aerosols can exhibit a phase separated morphology (e.g., but not limited to Ruehl et al.,
154 2012; Ruehl et al., 2016; Freedman, 2017; Kang et al., 2020; Malek et al., 2023). However,
155 inorganic salts may also enhance organic dissolution, known as “salting in” (Riva et al., 2019).
156 For instance, studies have observed increased diffusion in viscous SOA particles through the
157 aqueous droplet phase in the presence of inorganic salts (Reid et al., 2018; Jeong et al., 2022;
158 Sheldon et al., 2023). Increased diffusion is a result of salts disrupting the hydrogen bonding
159 network between neighboring organic molecules (Reid et al., 2018; Jeong et al., 2022; Sheldon et
160 al., 2023). Therefore, organic physicochemical properties (surface-activity, viscosity) of SOA,
161 such as 2-MT and 2-MTS, must be better defined to better predict mixed SOA/AS aerosol CCN
162 activity. To our knowledge there are no studies to date that investigate 2-MT and 2-MTS aerosol
163 water uptake, water uptake of mixtures with AS, and the potential effect of physicochemical
164 properties on CCN activity predictions.

165 In this study, we investigated the surface activity, diffusivity, droplet growth and water uptake of
166 2-MT, 2-MTS, and their mixtures with AS. 2-MT and 2-MTS surface tension values were
167 experimentally determined. A previous study by Ekström et al. (2009) found 2-MT to be
168 moderately surface-active. However, the surface activity of 2-MTS has not been characterized and
169 potential organic surface tension depression in the presence of AS has not been explored for both
170 organics. In tandem with surface tension measurements, this study estimated diffusion coefficients
171 of both compounds to explore the effects of viscosity and diffusivity on aerosol water uptake.
172 Aerosol κ -hygroscopicity for pure organic and organic-AS mixtures were experimentally
173 determined under both subsaturated conditions ($< 100\%$ RH) and supersaturated ($> 100\%$ RH)
174 conditions to observe both droplet growth and CCN activity, respectively. κ -hygroscopicity
175 measurements were then compared to κ -Köhler hygroscopicity theory to evaluate the efficacy of
176 traditional full dissolution and negligible viscosity assumptions in predicting the CCN activity of
177 both compounds and their mixtures. Lastly, Atomic Force Microscopy (AFM) measurements on
178 mixed particles were conducted to further understand particle morphology. The following work
179 provides a comprehensive analysis of the wide range of physicochemical properties that may
180 influence the droplet growth of 2-MT and 2-MTS mixed with AS.

181

182 **2. Experimental Methods**

183 2.1. Experimental Chemicals

184 For this study, ammonium sulfate (AS, $(\text{NH}_4)_2\text{SO}_4$; Thermo Fisher Scientific, $>99.0\%$), was
185 purchased and used without further purification. 2-methyltetrol (2-MT) and 2-methyltetrol sulfate
186 (2-MTS) samples were synthesized using the published procedure of Cui et al. (2018). 2-MT was
187 determined to be $> 98\%$ pure. The purity of 2-MTS was determined to be $\sim 73\%$ wt%, with remaining
188 sample mass estimated to be 3 wt% AS and 24 wt% sodium methyl sulfate (SMS). It should be

189 noted that from hereon 2-MTS sample refers to prescribed synthesized mixture and subsequent
190 calculations account for the estimated contributions of AS and SMS.

191 2.2. Surface Tension Measurements

192 The surface tension of 2-MT, 2-MTS, and their mixtures with AS was measured at atmospherically
193 relevant aqueous phase concentrations. Due to the limited amounts of synthesized sample, mixed
194 amounts were judiciously selected to mimic mixture ratios previously reported in the literature.
195 Specifically, a study by Cope et al. (2021) found that 2-MT concentrations in the atmosphere
196 reached an upper bound of 300 mM. Therefore, stock solutions of 300 mM 2-MT and 2-MTS were
197 prepared using deionized (DI) water. Furthermore, it is assumed that surface tension measurements
198 at dilutions higher than 300 mM are also relevant for droplet growth. A study Bain et al. (2023)
199 found that aerosol surface tension can be approximated from surface tension measurements of bulk
200 mixtures composed of < 100 mM organic component. Additionally, recent studies (Mikhailov et
201 al., 2024; Ferdousi-Rokib et al., 2025) also support the application of more dilute concentration
202 regimes to predict droplet growth. A recent study by Mikhailov et al. (2024) found that surface
203 tension depression observed in bulk dilute surface tension measurements was reflective of aerosol
204 properties. Ferdousi-Rokib et al. (2025) also found that salting out effects can be approximated in
205 mixtures having < 100 mM organic component. Thus, in this work, the stock solutions were diluted
206 to a 3-94 mM range; each stock solution and subsequent dilution concentrations are provided in
207 Supplemental Tables S1-S5.

208 Droplet surface tension ($\sigma_{s/a}$) was measured using a pendant drop tensiometer with a modified
209 profile analysis tensiometer (SINTERFACE Inc.); the experimental set up has been described in
210 Fertil et al. (2025). Briefly, the pendant drop tensiometer generates a droplet of solution (< 10 μ L)
211 suspended from a 0.9-mm diameter needle (Beier et al., 2019; Fertil et al., 2025). Droplets remain
212 suspended for 300 s to reach equilibrium; at each time step (\sim 1 s), the droplet $\sigma_{s/a}$ was obtained
213 from fitting the droplet curvature to the Young-Laplace Equation (Fordham & Freeth, 1948; Spelt,
214 1996; Padró et al., 2010). Surface tension measurements were run in triplicate; prior to each
215 measurement, the tensiometer was flushed with DI water and \sim 2 mL of solution. Measurements
216 were obtained at ambient room conditions, with temperature range of 20.2-22 $^{\circ}$ C and relative
217 humidity range of 40-45 % RH.

218 As the droplet equilibrates, surface tension changes, which is attributed to the accumulation of
219 solute diffusing to the droplet surface (Joos & Rillaerts, 1981; Eastoe et al., 1998; Chernyshev &
220 Skliar, 2015). As the solute saturates the surface, surface tension reaches equilibrium (Ross, 1945).
221 The accumulation of solute at the surface and resulting concentration gradient within the droplet
222 can be described by Fick's Second Law:

$$223 \quad \frac{\partial C}{\partial t} = D_s \frac{\partial^2 C}{\partial x^2}, \quad (1)$$

224 where concentration over time $\frac{\partial C}{\partial t}$ is proportional to the second derivative concentration over
225 position $\frac{\partial^2 C}{\partial x^2}$ and the diffusion coefficient D_s ($m^2 s^{-1}$). The dynamic surface tension can be correlated
226 with solute diffusion over time as (Joos & Rillaerts, 1981):

227
$$\sigma_t = \sigma_0 - 2RTC \left(\frac{D_s t}{\pi} \right)^{0.5}, \quad (2)$$

228 where σ_0 is the starting surface tension, σ_t is the surface tension at specified time t , R is the universal
229 gas constant, T is temperature, and C is organic molar concentration. Here, evaporation effects are
230 negligible during the short suspension times. Therefore, the organic molar concentration C is
231 equivalent to the droplet solution concentration as Eq. 2 can then be rearranged to solve for D_s
232 using dynamic surface tension measurements.

233

234 2.3. Aerosol Experimental Methods

235 2.3.1. Aerosol Generation

236 Solutions of 0.1 g L⁻¹ total solute (2-MT, 2-MTS, and mixtures with AS) were prepared using
237 ultra-purified Millipore water (18 MΩ·cm). Mixtures compositions are provided in Table S6.
238 Polydisperse aerosols were then generated by passing each aqueous solution through a constant
239 output Collison Nebulizer (Atomizer, TSI 3076); the generated aerosols were then dried to < 5%
240 RH using two silica gel dryers in series. Aerosols were then analyzed for their water uptake
241 properties under sub- and supersaturated conditions. To determine aerosol phase morphology,
242 atomic force microscopy (AFM) images were also obtained. In addition to water uptake and AFM
243 measurements, organic density and shape factor were measured; for details on density and shape
244 factor measurements, see Armstrong et al. (2025).

245 2.3.2 Water Uptake Measurements

246 A humidified tandem differential mobility analyzer (H-TDMA) measured droplet growth under
247 subsaturated conditions. Dry, polydisperse aerosols were size selected at 100, 150, and 200 nm by
248 an electrostatic classifier (DMA 1, TSI 3082; flow rate = 0.3 L min⁻¹) and humidified using a
249 Nafion humidification line (PermaPure M.H. series); particles were humidified at 88.2% ± 1.5%
250 RH. Selected dry diameters are often assumed to be spherical, thus having a shape factor (χ) of 1
251 (DeCarlo et al., 2004). Aerodynamic aerosol classifier (AAC) shape factor measurements
252 confirmed 2-MT and 2-MTS sphericity (Armstrong et al., 2025). The wet diameter (D_w) was
253 measured using a second electrostatic classifier (DMA 2, TSI 3082; flow rate = 0.3 L min⁻¹); the
254 ratio of D_w to the dry-size selected diameter (D_d) is equal to the growth factor (G_F). The
255 experimental set up is provided in Fig. S1. To calibrate the H-TDMA, a 0.1 g L⁻¹ solution of AS
256 was aerosolized; dried AS aerosols were size selected at 100 and 150 nm. Dried AS aerosol G_F
257 and instrument RH was measured, with calibration measurements repeated multiple times as
258 reported in Table S7. The experimental solutions were then aerosolized, and G_F was obtained for
259 each solution; G_F is used to calculate the hygroscopicity parameter under subsaturated conditions,
260 $\kappa_{\text{H-TDMA}}$. In addition to subsaturated conditions, water uptake was measured under supersaturated
261 (SS) conditions using a CCNC-100 (Droplet Measurement Technologies); the experimental set up
262 is provided in Fig. S2. The theory and operation of the CCNC has been previously described
263 (Roberts & Nenes, 2005; Lance et al., 2006; Rose et al., 2008). The Scanning Mobility CCN
264 Analysis (SMCA) protocol was used to measure droplet activation (Moore et al., 2010). Briefly,
265 the dried polydisperse aerosols were passed through an electrostatic classifier (TSI 3080) in

266 scanning mode and charged; scanning mode operated from 8-352 nm for 135 s. The DMA operated
267 at a sheath-to-aerosol flow rate ratio of 10:1, and aerosol sample flow rate of 0.8 L min⁻¹. The
268 monodisperse, size-selected aerosol stream was then sampled by a condensation particle counter
269 (CPC, TSI 3776, flow rate = 0.3 L min⁻¹) and the CCNC-100 (flow rate = 0.5 L min⁻¹) in parallel.
270 The CPC counted the number concentration of dry particles at a given particle size (condensation
271 nuclei, N_{CN}). The CCNC exposed the particles to 0.3-1.4%SS and the number concentration of
272 particles activated (N_{CCN}) were measured. The instrument set up was calibrated using AS (Rose et
273 al., 2008) and the calibration data are provided in Table S8 and Fig. S3.

274 The CPC counted the number concentration of dry particles at a given particle size (condensation
275 nuclei, N_{CN}). The CCNC exposed the particles to 0.3-1.4%SS and the number concentration of
276 particles activated (N_{CCN}) were measured. The instrument set up was calibrated using AS (Rose et
277 al., 2008) and the calibration data are provided in Table S8 and Fig. S3.

278 CCN data of AS and experimental solutions were analyzed using the Python-based CCN Analysis
279 Toolkit (PyCAT 1.0) (Gohil, 2022; Gohil & Asa-Awuku, 2022). PyCAT is a Python version of
280 SMCA and is available on GitHub for public use. The analysis toolkit calculated the activation
281 ratio N_{CCN}/N_{CN} for each dry particle size. The activation ratios were fitted using a sigmoid curve
282 and the critical diameter ($D_{p, 50}$) was found, at which ~50% of the dry particles activate. A charge
283 correction is applied in PyCAT using the multi-charge correction algorithm previously described
284 (Fuchs, 1963; Wiedensohler, 1988). The obtained critical diameter of each solution is then used to
285 calculate the single hygroscopicity parameter under supersaturated conditions, κ_{CCN} .

286 2.3.3. Atomic Force Microscopy (AFM) Morphology

287 Atomic force microscopy (AFM) measurements were utilized to characterize aerosol phase
288 morphology. 2-MTS, 2-MTS/AS, and 2-MT/AS particles were collected onto silicon substrates
289 (Silson Ltd) using a cascade impactor (Sioutas Cascade Impactor, flow rate = 9 L min⁻¹ and stored
290 at room temperature and relative humidity (40-50% RH) prior to analysis. Imaging followed the
291 procedure of Zhang et al. (2018). Briefly, particles were imaged in a 5 x 5 μm region using a
292 Dimension ICON® AFM (Bruker) in tapping mode with resonant frequency of 150 kHz and spring
293 constant of 5.4 N m⁻¹.

294 2.3.4 Viscosity and Diffusion Calculation

295 The viscosity and the diffusion coefficients of the 2-MT and 2-MTS aerosols were calculated using
296 a modified Vogel-Tammann-Fulcher (VTF) equation (DeRieux et al., 2018). The dry glass
297 transition temperature values were determined to be 226 K and 276 K from a previous study by
298 Zhang et al. (2019b). The Gordon-Taylor coefficient and the fragility coefficient were assigned as
299 2.5 and 20, respectively. The hygroscopicity values were used from the measurement of H-TDMA
300 of this study.

301

302 3. Traditional κ -Köhler theory

303 Traditionally, water uptake of aerosol particles has been calculated using κ -Köhler theory (Köhler,
 304 1936; Petters & Kreidenweis, 2007). Köhler theory considers aerosol physicochemical properties
 305 (e.g., solute density, molecular weight) to describe the equilibrium water vapor saturation ratio at
 306 a droplet's surface (S_{eq}). The equilibrium relationship encompasses two competing effects. The
 307 Kelvin effect describes the increase of water vapor saturation as a result of the curvature of the
 308 droplet; the Kelvin effect is represented by droplet surface tension $\sigma_{s/a}$. The Raoult (solute) effect
 309 competes by decreasing vapor pressure due to the presence of solute in the aqueous droplet; the
 310 solute effect is represented by the water activity term, a_w (Seinfeld & Pandis, 1998; Wex et al.,
 311 2008). For compounds dissolved in water, water activity can be parameterized by the single
 312 hygroscopicity parameter, κ , as follows (Petters & Kreidenweis, 2007; Sullivan et al., 2009):

$$313 \quad \frac{1}{a_w} = 1 + \kappa \frac{V_s}{V_w}, \quad (3)$$

314 where V_w and V_s are the volume of water and dry solute, respectively. Therefore, the equilibrium
 315 saturation ratio (S_{eq}) over the droplet is described as:

$$316 \quad S_{eq} = \left(1 + \kappa \frac{D_d^3}{D_w^3 - D_d^3}\right)^{-1} \exp\left(\frac{4\sigma_{s/a}M_w}{RT\rho_w D_d}\right), \quad (4)$$

317 where ρ_w is the density of water, M_w is the molecular weight of water, R is the universal gas
 318 constant and T is the temperature.

319 κ describes ability of an aerosol to uptake water assuming full dissolution, and can be calculated
 320 from the intrinsic properties of the solute as κ_{int} (Sullivan et al., 2009):

$$321 \quad \kappa_{int} = \frac{v_s \rho_s M_w}{\rho_w M_s}, \quad (5)$$

322 where M_s is the molecular weight of solute, v_s is the van't Hoff factor, and ρ_s is the density of the
 323 solute; Armstrong et al. (2025) found 2-MT and 2-MTS density to be 1.4 g cm⁻³ and 2.46 g cm⁻³,
 324 respectively. To estimate κ -hygroscopicity of aerosols containing more than one compound, the
 325 Zdanovskii, Stokes, and Robinson (ZSR) mixing rule can be applied to estimate (Petters &
 326 Kreidenweis, 2007):

$$327 \quad \kappa_{ZSR} = \sum_i \varepsilon_i \kappa_i, \quad (6)$$

328 where ε_i is the volume fraction of the individual solute component, i .

329 Experimental data can be used to derive aerosol κ . Under subsaturated (< 100% RH) conditions,
 330 G_F is related to hygroscopicity as follows (Kreidenweis & Asa-Awuku, 2014):

$$331 \quad \kappa_{H-TDMA} = \frac{(G_F^3 - 1)}{RH} - G_F^3 + 1, \quad (7)$$

$$\frac{\exp\left(\frac{4\sigma_{s/a}M_w}{RT\rho_w D_d G_F}\right)}$$

332 Where κ_{H-TDMA} is subsaturated hygroscopicity and RH is the relative humidity of the H-TDMA
 333 instrument as a decimal. Similarly, for supersaturated (>100% RH), the critical diameter correlates
 334 to κ as follows (Petters & Kreidenweis, 2007):

335
$$\kappa_{\text{CCN}} = \frac{4 \left(\frac{4\sigma_{s/a} M_w}{RT\rho_w} \right)^3}{27D_{p,50}^3 \ln^2 SS'} \quad (8)$$

336 Where κ_{CCN} is supersaturated hygroscopicity. It is assumed that droplet surface tension $\sigma_{s/a}$ is
 337 equivalent to that of the surface tension of water $\sim 72 \text{ mN m}^{-1}$. Köhler theory also assumes that all
 338 solutes are well mixed within the aqueous phase. The Köhler/ZSR model does not account for
 339 potential viscosity and diffusivity limitations due to inorganic-organic mixing in the aqueous
 340 phase. Therefore, in this study, κ - Köhler values are predicted assuming both 2-MT and 2-MTS
 341 are well mixed within the aqueous phase and fully contribute to droplet growth. The applicability
 342 of these assumptions is discussed in the later sections. Additionally, a list of variable abbreviations
 343 is provided in Table S9.

344

345 4. Results

346 4.1. Surface Tension and Diffusion

347 *Organic Samples*

348 Dynamic pendant drop tensiometer measurements were taken for 2-MT and 2-MTS samples;
 349 measurements were performed by hanging droplets $< 10 \mu\text{L}$ over a period of 300 s. The droplet
 350 curvature was measured every 1 s. Average surface tension values were obtained for 2-MT and 2-
 351 MTS when droplet surface tension values remained constant (at equilibrium) and are listed in
 352 Table S10 and shown in Fig. 1.

353 In the dilute bulk measurement regime, 2-MT sample (Fig. 1, orange squares) and 2-MTS sample
 354 (Fig. 1, purple closed circles) $\sigma_{s/a}$ values are close to pure water ($\sim 72 \text{ mN m}^{-1}$, Fig. 1, blue dashed
 355 line). For solutions $< 53 \text{ mM}$ organic concentration, 2-MT and 2-MTS samples exhibit little to no
 356 surface-activity. Surface-activity is similar to the dilute surface tension of pure AS, a non-surface-
 357 active compound, which remains $\sim 72 \text{ mN m}^{-1}$ (Fig. 1, red circles, Pruppacher et al., 1997).
 358 However, for organic solutions $> 53 \text{ mM}$, minimal surface tension depression is observed with $\sigma_{s/a}$
 359 values between $\sim 68\text{--}70 \text{ mN m}^{-1}$ (Fig. 1 and Table S10); in comparison, AS surface tension
 360 increases with concentration, as observed in Fig. 1 and with previous studies (namely, Pruppacher
 361 et al., 1997; Hyvärinen et al., 2005; Mikhailov et al., 2024). Therefore, both synthesized 2-MT and
 362 2-MTS sample mixtures can be classified as weakly surface-active. A previous study by Riva et
 363 al. (2019) observed greater surface tension depression for IEPOX SOA/sulfate mixtures. In
 364 particular, enhanced surface tension depression was attributed to organic partitioning and
 365 formation of 2-MT and 2-MTS oligomers (Riva et al., 2019).

366 In comparison to the surface tension of other short-chained particulate organosulfates, such as
 367 sodium ethyl sulfate (Fig.1, black triangles) and sodium methyl sulfate (Fig. 1, grey triangles), 2-
 368 MT and 2-MTS have lower dilute surface values (Peng et al., 2021). However, similar to other
 369 surface-active organosulfates (sodium ethyl sulfate and sodium octyl sulfate), neither 2-MT
 370 sample and 2-MTS sample surface tension significantly depress aerosol surface tension (Table S11
 371 and S14). For example, Mikhailov et al. (2024) observed surface tension depression as low as \sim

372 56 mN m⁻¹ for dilute D-glucose/AS mixtures. Furthermore, moderately surface-active compounds,
 373 such as 2-methylglutaric acid (2-MGA, Fig. 1, green squares) and sodium octyl sulfate (Fig. 1,
 374 grey diamonds) exhibit surface tension depression in the range of ~ 64-68 mN m⁻¹ for
 375 concentrations ≤ 22 mM (Tables S13-S14). Additionally, stronger surface-active organics
 376 (surfactants), such as sodium dodecyl sulfate (SDS) show surface tension at the droplet surface
 377 can be depressed in the dilute regime. SDS reaches $\sigma_{s/a}$ of ~ 39 mN m⁻¹ at 9 mM organic (Fig. 1
 378 and Table S15). Sodium octyl sulfate, SDS, and 2-MGA present noticeable surface tension
 379 depression in the dilute bulk measurement regime (Fig. 1) that affect aerosol properties
 380 (Vepsäläinen et al., 2023; Zhang et al., 2023; Kleinheins et al., 2025). However, in comparison to
 381 previously studied organics, 2-MT and 2-MTS $\sigma_{s/a}$ samples remain close to pure water in the dilute

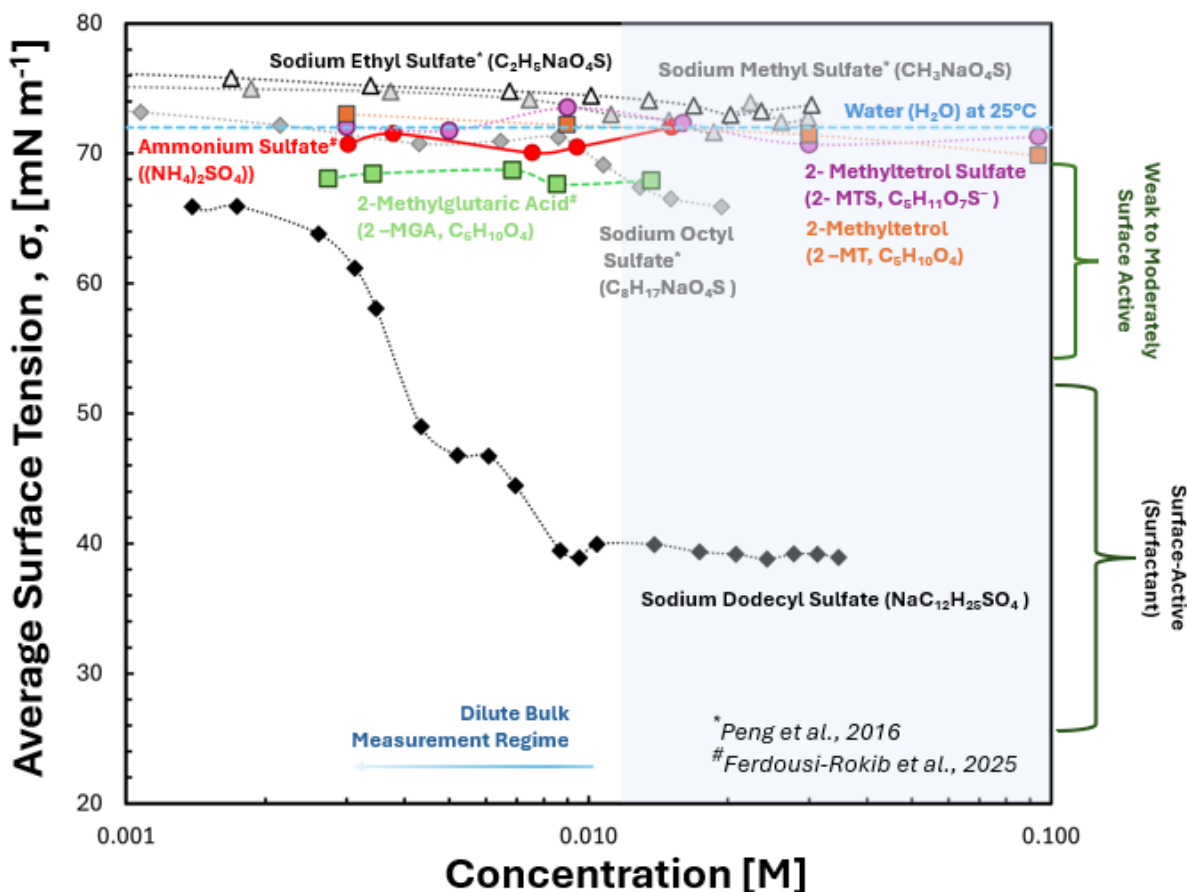


Figure 1. Experimental average surface tension $\sigma_{s/a}$ values of compounds as a function of concentration. Average equilibrium surface tension of synthesized 2-MT (>98 wt% purity) and 2-MTS (~73 wt% purity) samples are shown as closed orange squares and closed purple circles, respectively. The surface tension of the organosulfates, including sodium ethyl sulfate (black open triangles), sodium methyl sulfate (grey closed triangles), and sodium octyl sulfate (grey closed diamonds) were obtained by Peng et al. (2016). 2-methylglutaric acid (green closed squares) and ammonium sulfate (red closed circles) $\sigma_{s/a}$ were obtained from Ferdousi-Rokib et al., 2025 (in review). Sodium dodecyl sulfate (SDS) $\sigma_{s/a}$ is shown as black diamonds. Pure water $\sigma_{s/a}$ at 25°C (~ 72 mN m⁻¹) is represented as a dashed blue line. Compounds can be categorized as weak to moderately surface active (65-75 mN m⁻¹) or surface-active (surfactants, < 65 mN m⁻¹) for compounds that can depress surface tension below that of pure water. Bain et al 2023 consider the dilute bulk measurement regime to be less than 100mM.

382 bulk regime (Fig. 1). Previous studies by Bain et al. (2023) and Werner et al. (2025) emphasize
383 the role of surface area-to-volume ratio dictating aerosol surface tension. Specifically, aerosol
384 surface tension values are best represented by surface tension measurements of the organic in bulk
385 solutions < 100 mM (Bain et al., 2023; Ferdousi-Rokib et al., 2025; Werner et al., 2025). Thus, 2-
386 MT and 2-MTS sample mixture surface activity is negligible for droplet activation as both dilute
387 organic $\sigma_{s/a}$ is close to that of pure water (~ 72 mN m⁻¹).

388 It should be reiterated and noted that the synthesized 2-MTS sample is 73% pure 2-MTS and is
389 likely mixed with AS and SMS. Both SMS and AS (Fig.1, red circles; Table S16) have surface
390 tension values, > 72 mN m⁻¹ in the dilute regime. However, despite the presence of impurities in
391 the mixture, synthesized 2-MTS sample mixture surface tension reaches values ~ 68 mN m⁻¹.
392 Therefore, the presence of these impurities may counteract possible further surface tension
393 depression exhibited by pure 2-MTS. Future work can better probe surface tension of the pure
394 organic 2-MTS and effects of SMS by applying a multicomponent surface tension model (e.g.,
395 multicomponent models of Topping et al., 2007) to dynamic surface tension measurements.

396 Both 2-MT and 2-MTS are considered viscous compounds and may diffuse slowly through the
397 measured droplets (Reid et al., 2018; Zhang et al., 2019a; Chen et al., 2023). As a result,
398 equilibrium surface tension is reached after a period of time, t . The rate of diffusion of the organic
399 through water, also known as the diffusion coefficient D_s , can be calculated from dynamic surface
400 tension measurements (Eq. 1-2). Diffusion coefficient values for synthesized 2-MT and 2-MTS
401 samples range between 10^{-9} to 10^{-11} m² s⁻¹, with diffusion slowing with increasing sample
402 concentration. Specifically, D_s for the 2-MT and 2-MTS samples are estimated to be 10^{-9} to 10^{-11}
403 m² s⁻¹ and 10^{-9} to 10^{-10} m² s⁻¹, respectively (Table S17). Additionally, the viscosity-based diffusion
404 coefficient was calculated and shown in Table S19. 2-MT and 2-MTS diffusion rates are
405 comparable to rates observed for other previously investigated viscous components in aqueous
406 solution (Curry et al., 2018; Tandon et al., 2019). For example, methylglyoxal, a known viscous
407 component, has an aqueous phase diffusion rate $\sim 10^{-9}$ m² s⁻¹ (Curry et al., 2018). In addition to
408 the diffusion coefficients in aqueous solution, a study by Chenyakin et al. (2017) average diffusion
409 coefficients between 10^{-13} and 10^{-14} m² s⁻¹ for organic molecules in a sucrose-water proxy for SOA.
410 A study by Renbaum-Wolff et al. (2013) reported diffusion coefficients ranging from 10^{-13} and 10^{-15}
411 m² s⁻¹ for α -pinene-derived SOA between 70-90% RH. Indeed, 2-MT and 2-MTS have been
412 previously observed to be highly viscous, resulting in slow diffusivity (Wang et al., 2011;
413 Chenyakin et al., 2017; Tandon et al., 2019; Zhang et al., 2019a; Chen et al., 2023). Furthermore,
414 at higher viscosity and lower diffusion rates, the diffusion of solute molecules fails to follow the
415 Stokes-Einstein relationship describing the self-diffusion of solute molecules through a liquid
416 phase (Einstein, 1905; Chenyakin et al., 2017; Tandon et al., 2019). For viscous material, such as
417 2-MT and 2-MTS sample, diffusion in water is self-limited (Chenyakin et al., 2017). Slow
418 diffusion correlates with the longer time scales needed to reach equilibrium surface tension for
419 more concentrated sample solutions; the solute molecules are limited in their ability to accumulate
420 to the surface; thus, time is an important factor in the surface tension measurements. This effect is
421 more prominent in 2-MT than 2-MTS sample, as evident in its slower diffusion rates for
422 concentrations > 30 mM (Table S17).

424 Previous studies have observed that inorganic compounds, such as AS, mixed with organics can
 425 enhance surface tension effects (Topping, 2010; El Haber et al., 2023). Additionally, AS can result
 426 in the partitioning of organics to the to the surface (i.e., the movement of organics to the surface is
 427 commonly referred to as salting-out). To determine if partitioning effects are present in organic/AS
 428 mixtures, synthesized 2-MT and 2-MTS samples were mixed with 500 mM AS and dynamic
 429 surface tension measurements were taken; mixture dynamic surface tension measurements are
 430 shown in Fig. 2. Average mixed surface tension values are listed in Table S10.

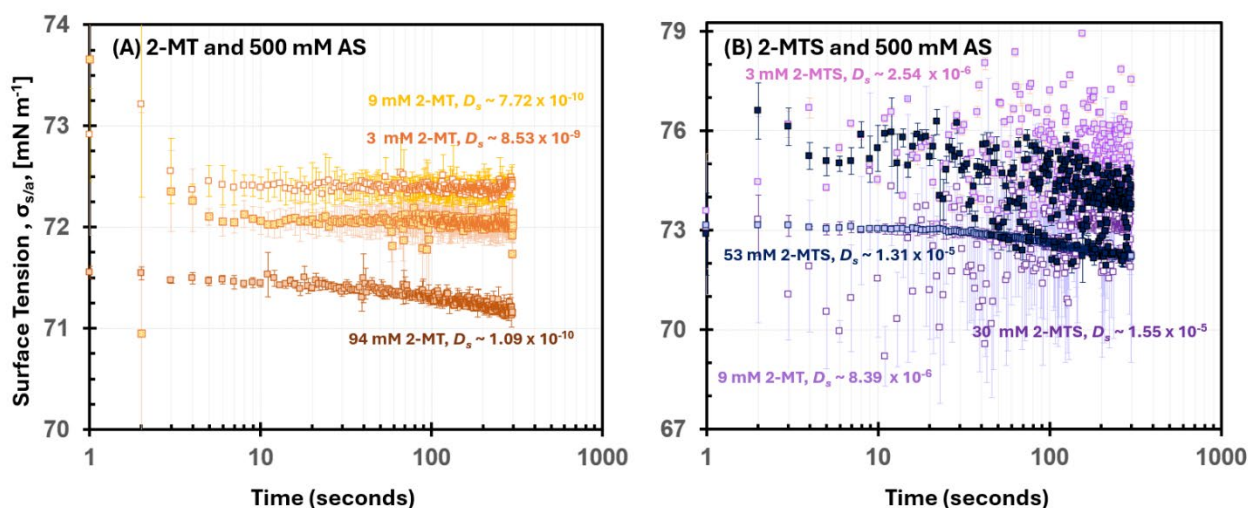


Figure 2. Dynamic $\sigma_{s/a}$ measurements for (A) 3-94 mM 2-MT sample/500 mM AS and (B) 3-53 mM 2-MTS sample/500 mM AS mixtures. Dynamic $\sigma_{s/a}$ was recorded over a duration of 300 seconds. The 2-MTS sample mixtures likely contain additional contributions of AS (3 wt%) and SMS (24 wt%), which may further influence dynamic surface tension measurements and overall sample diffusivity.

431 For mixtures of 3-9 mM 2-MT and 500 mM AS, surface tension remains stable $\sim 75 \text{ mN m}^{-1}$ and
 432 is higher than 2-MT (>98 wt% purity) solution surface tension alone (Fig. 2A). Higher $\sigma_{s/a}$ values
 433 indicate a lack of salting out effects and organic surface partitioning; previous surface tension
 434 studies of organic/AS mixtures observed salting out effects through lower $\sigma_{s/a}$ values in comparison
 435 to pure organic solutions (Ferdousi-Rokib et al., 2025 (in review)). Thus, for 3-9 mM 2-MT with
 436 500 mM AS mixtures, organic partitioning is not enhanced, and the droplet surface tension aligns
 437 with pure AS $\sigma_{s/a}$ (Fig.1. and Table S16). When organic concentration in the mixture is increased
 438 to 94 mM, a stronger time dependence for surface tension is observed (Fig. 2A); an equilibrium
 439 surface tension of $\sim 71.2 \text{ mN m}^{-1}$ is reached at $\sim 300 \text{ s}$. This lower surface tension for 94 mM 2-MT
 440 with 500 mM AS compared to the previous 2-MT/AS mixture correlates with the higher
 441 concentration of organic in solution. However, the longer equilibrium time is indicative of a slow
 442 solute diffusion in the droplet.

443 Previous studies have observed diffusion effects within dynamic surface tension measurements
 444 and estimated solute diffusion (Eastoe et al., 1998; Bain et al., 2024). To determine organic
 445 diffusion within AS mixtures, the D_s was calculated using Eqs. 1-2. For 2-MT/AS mixtures, D_s

446 ranged from 10^{-9} to 10^{-11} , with diffusion slowing as organic concentration increases (Fig. 2A, Table
447 S17). 2-MT organic diffusion in AS mixtures is similar to that of the organic 2-MT solution (with
448 > 98% purity) D_s values. As a result, 2-MT organic diffusion remains relatively unaffected in the
449 presence of AS. The organic 2-MT molecules do not diffuse fast enough to fully accumulate at the
450 surface and substantially lower surface tension.

451 Similar to 2-MT/AS mixtures, 2-MTS/AS mixture surface tension was higher than 2-MTS sample
452 solution surface tension alone. 2-MTS/AS mixture $\sigma_{s/a}$ values ranged from ~ 72.5 to 75 mN m $^{-1}$
453 and remain close to surface tension values of pure AS. Furthermore, $\sigma_{s/a}$ values remain constant as
454 the 2-MTS organic concentration increases from 3 to 53 mM; the minimal correlation between
455 organic concentration and surface tension implies that AS dominates droplet surface tension at the
456 surface-air interface. In addition to being stable across organic concentrations. 2-MTS/AS $\sigma_{s/a}$
457 reaches equilibrium faster than 2-MT/AS; equilibrium is achieved across the mixtures at < 100 s
458 (Fig. 2B). Indeed, based on the dynamic surface tension measurements, D_s for 2-MTS within AS
459 mixtures remains $\sim 10^{-9}$, indicating slightly faster organic diffusivity through the droplet than 2-
460 MT (Table S17). In the presence of AS, D_s increases by an order of magnitude. This suggests the
461 presence of AS increases solubility and dispersion of 2-MTS molecules through the droplet, (Prisle
462 et al., 2010; Toivola et al., 2017). A similar phenomenon has been observed in glyoxal/AS mixtures
463 as the presence of the inorganic compound improves dissolution of the organic (Kampf et al.,
464 2013). Therefore, the higher 2-MTS/AS surface tension values and diffusivity indicate that the
465 organic is well dispersed within the droplet, but AS dominates droplet surface tension properties.
466 Both 2-MT and 2-MTS present complex viscous properties that may affect droplet phase and
467 potentially change in the presence of inorganic compounds, such as AS. It is important to note that
468 for 2-MTS, the remaining sample mass also contains SMS, which may further influence the
469 estimated diffusion rates (Vignes, 1966; Wallace et al., 2021). Diffusion coefficients within
470 aerosols may be sensitive to mixture ratio, as observed by Wallace et al. (2021). Thus, the presence
471 of SMS may affect the 2-MTS sample/AS diffusion rates observed in this study. Future work
472 should explore the influence of SMS on viscous organic diffusivity by applying this study's
473 methodology to a range of 2-MTS sample/SMS mixtures with 2-MTS contribution greater than 73
474 wt%. Ultimately, diffusion effects were observed through dynamic surface tension measurements
475 and may influence 2-MT, 2-MTS, and AS-mixed aerosol water uptake properties. Therefore,
476 additional diffusion effects on synthesized organic and organic/AS aerosol mixtures were probed
477 through the lens of water uptake measurements.

478

479 4.2. Water Uptake Measurements

480 In addition to the previous measurements, the droplet growth of 2-MT, 2-MTS samples, and their
481 respective AS mixtures were measured; hygroscopicity was estimated under both subsaturated and
482 supersaturated conditions. Mixtures were varied by sample wt% (Table S21); organic wt% of 2-
483 MTS is estimated by accounting for impurities present in the sample and their respective properties
484 (e.g., density, hygroscopicity, Table S20). The adjusted mass wt% for 2-MTS/AS mixtures are
485 listed in Table S21. For subsaturated hygroscopicity, the H-TDMA instrument setup was used to
486 measure G_F for all experimental solutions at 88.2% RH. Experimental growth factor values for 2-

487 MT/AS and 2-MTS/AS mixtures are listed in Tables S20-S21. For supersaturated hygroscopicity,
 488 the CCNC instrument setup was used to obtain experimental $D_{p,50}$ values across multiple
 489 supersaturation conditions (0.31, 0.43, 0.65, 0.88, 1.10, 1.32, and 1.54 % SS); the critical diameter
 490 values for 2-MT/AS and 2-MTS/AS mixtures are listed in Tables S22-S23. For 100 wt% 2-MTS
 491 hygroscopicity, impurity (SMS and additional AS) hygroscopicity are accounted for by applying
 492 ZSR mixing rule (Eq. 6) to solve for pure organic hygroscopicity; SMS κ was assumed to be ~ 0.459
 493 based on Peng et al. (2021).

494 Under subsaturated conditions, both 2-MT and 2-MTS are moderately hygroscopic, with κ_{H-TDMA}
 495 values of 0.103 and 0.276, respectively (Fig. 3A). For 2-MT/AS (Fig. 3A, orange open squares)
 496 and 2-MTS/AS (Fig. 3A, purple open circles) aerosol mixtures, subsaturated hygroscopicity values
 497 are similar. For 2-MT/AS mixtures ≤ 45 wt% organic, κ values plateau close to pure AS ($\kappa_{int} =$
 498 0.61) at a $\kappa_{H-TDMA} \sim 0.56$. For mixtures > 45 wt% organic, both 2-MT and 2-MTS exhibit lower κ_{H-}

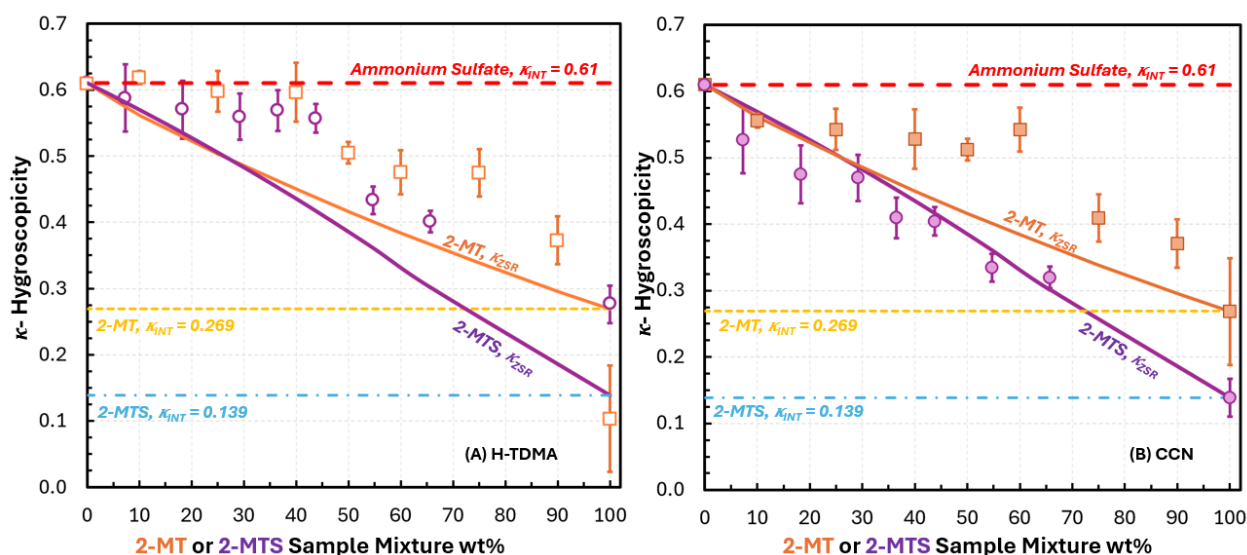


Figure 3. Experimental κ -hygroscopicity measurements derived from (A) H-TDMA measurements and (B) CCNC measurements. 2-MTS/AS sample mixture wt% was adjusted based on the presence of AS and SMS impurities (Table S21). Subsaturated hygroscopicity (κ_{H-TDMA}) of 2-MT/AS and 2-MTS /AS sample mixtures are represented as open orange squares and open purple circles, respectively. Supersaturated hygroscopicity (κ_{CCN}) for 2-MT/AS and 2-MTS sample/AS mixtures are represented as orange squares and purple circles, respectively. For 100 wt% 2-MTS, κ values were adjusted to account for impurities by applying mixing rule, assuming an SMS κ of ~ 0.459 and AS $\kappa \sim 0.61$ (Eq. 6, Table S20). κ -Köhler theory (κ_{ZSR}) was used to predict hygroscopicity of 2-MT/AS (solid orange line) and 2-MTS sample/AS (solid purple line) via Eq. 6. Organic κ_{int} was determined from 100 wt% κ_{CCN} . 2-MT κ_{int} (yellow dashed line) was determined to be 0.269. 2-MTS κ_{int} (blue dashed line) was determined to be 0.139.

499 κ_{TDMA} values, ranging from 0.103-0.505 for 2-MT/AS mixtures and 0.276–0.433 for 2-MTS/AS
 500 mixtures. Previous studies by Malek et al. (2023) and Ferdousi-Rokib et al. (2025) have observed
 501 a plateau in hygroscopicity for AS-dominated organic mixtures prior to a decrease in κ due to the
 502 presence of phase separated morphology; as a result of phase separation, the inorganic AS remains
 503 dissolved in the aqueous phase and drives hygroscopicity (Malek et al., 2023). After a threshold
 504 composition is reached (45 wt% organic), more organic solute contributes to the aqueous phase
 505 and thus hygroscopicity is lowered.

506 Under supersaturated conditions, 2-MT and 2-MTS samples remain moderately hygroscopic, with
507 κ_{CCN} being 0.269 and 0.139, respectively. For 2-MT/AS sample mixtures (Fig. 3B, closed orange
508 squares), supersaturated κ mimics the same trend as subsaturated 2-MT/AS κ ; for mixtures ≤ 60
509 wt% 2-MT, κ_{CCN} also shows a plateau at ~ 0.53 and then decreases with increased organic aerosol
510 composition. In comparison, the 2-MTS/AS sample mixtures (Fig. 3B, purple circles) present a
511 linear hygroscopic trend; as organic wt% increases, κ_{CCN} drops in a linear fashion resembling ideal
512 mixing and volume additivity (Petters & Kreidenweis, 2007). Indeed, 2-MTS/AS κ_{CCN} correlates
513 with the hygroscopicity trend predicted by κ_{ZSR} values (Eqs. 11-12) (Fig. 3B, purple line). 2-
514 MTS/AS supersaturated hygroscopicity agrees well with original Köhler theory ($R^2 = 0.972$, Table
515 S26), suggesting full 2-MTS dissolution and contribution to water uptake. By contrast, 2-MT/AS
516 mixtures do not agree with κ -Köhler theory ($R^2 = 0.787$, Table S26), with the greatest discrepancy
517 observed in the region between the κ experimental plateau and κ_{ZSR} (Fig. 3, orange line);
518 additionally, subsaturated 2-MTS/AS mixtures deviate from κ_{ZSR} during the initial hygroscopic
519 plateau (Fig. 3A, purple line). Thus, for 2-MT/AS mixtures and subsaturated 2-MTS/AS aerosols,
520 the ideal volume additive mixing rule does not apply. This can once again be attributed to
521 limitations to organic dissolution into the aqueous phase (Malek et al., 2023). For 2-MTS/AS
522 sample mixtures, both subsaturated and supersaturated hygroscopic trends may be further
523 impacted by the presence by SMS. The contributions of AS and SMS hygroscopicity are accounted
524 for 2-MTS sample mixture. κ was estimated using ZSR mixing rule, which assumes ideal
525 interactions between SMS, AS, and 2-MTS. However, non-idealities (e.g., phase separation,
526 salting in) may result in SMS having a greater influence on hygroscopicity and can be the focus of
527 future exploration.

528 In addition to non-ideal hygroscopic trends, it is noted that overall, κ_{CCN} values remain lower than
529 κ_{H-TDMA} values for both 2-MT/AS and 2-MTS/AS sample mixtures, contrary to the usual trend of
530 $\kappa_{CCN} > \kappa_{H-TDMA}$ (Petters & Kreidenweis, 2007). The observed difference suggests greater organic
531 dissolution and contribution to hygroscopicity in the supersaturated regime compared to
532 subsaturated conditions. This suggests potential viscosity and diffusion limitations on
533 hygroscopicity as RH transitions from sub- to supersaturated. Indeed, the viscosity of the 2-MT
534 and 2-MTS changes under different conditions. Both compounds remain in the semi-solid phase
535 state before entering the CCNC, and behave like liquids in the H-TDMA, as shown in Table S18.
536 Additionally, Asa-Awuku and Nenes (2007) report diffusivity limitation effects on aerosol water
537 uptake for compounds with D_s values $\leq 2.5 \times 10^{-10}$, well within the range of D_s values for 2-MT,
538 and 2-MT sample/AS. Water uptake was shown to be driven by the viscous organic phase slowly
539 diffusing into the aqueous phase (Asa-Awuku & Nenes, 2007). Thus, it is believed that both 2-MT
540 and 2-MTS slowly dissolve and phase separate to form a viscous phase under subsaturated
541 conditions, corresponding to slow diffusion coefficients. AS is an inorganic compound that is
542 assumed to instantaneously dissolve into the aqueous phase and thus drives hygroscopicity when
543 the droplet is phase separated, such as for 2-MT/AS mixtures (Fig. 2). However, lower κ values at
544 supersaturated conditions can be attributed to higher water content; previous studies have found
545 greater water content correlating with reduced viscosity due to a plasticizing effect and resulting
546 in enhanced organic mixing (O'Meara et al., 2016; Reid et al., 2018; Jeong et al., 2022). Thus, the
547 organic viscous phase may experience “cracking” and greater movement of organic molecules
548 through the aqueous phase (Tandon et al., 2019). Therefore, phase behavior of the organic can

549 have a strong influence on aerosol water uptake. Additionally, the non-ideal hygroscopic behavior
550 of 2-MT/AS and subsaturated 2-MTS/AS mixtures versus the ideal hygroscopic behavior of
551 supersaturated 2-MTS/AS aerosols can be probed through imaging of the aerosol mixture phase
552 behavior.

553

554 4.3. Phase Morphology

555 To further understand the phase state and morphology of 2-MT and 2-MTS sample mixtures with
556 AS, AFM images were taken at varied organic wt% (Fig. 4). Dried synthesized 2-MTS presents
557 itself as a viscous, spherical particle, indicated by its smooth surface (Fig. S4); this agrees with
558 both shape factor measurement of ~ 1 (Armstrong et al., 2025 (2025)) and diffusion coefficient
559 values. As inorganic AS is mixed with 2-MTS sample, phase behavior changes. At 10 wt% 2-MTS
560 sample (Fig. 4B), particles exhibit an engulfed core-shell morphology. A previous study by Cooke
561 et al. (2022) observed a similar core-shell morphology for AS-seeded IEPOX-derived SOA
562 particles; the study observed an organic shell, while the inorganic salt was observed to be present
563 in the shell as well as within an aqueous core (Cooke et al., 2022). With AS dispersed on the outer
564 shell as well as being present in an aqueous core, the inorganic salt in the shell will likely easily
565 dissolve during water uptake and drive hygroscopicity, consistent with the results as observed in
566 subsaturated hygroscopicity measurements. However, AS within the shell may introduce

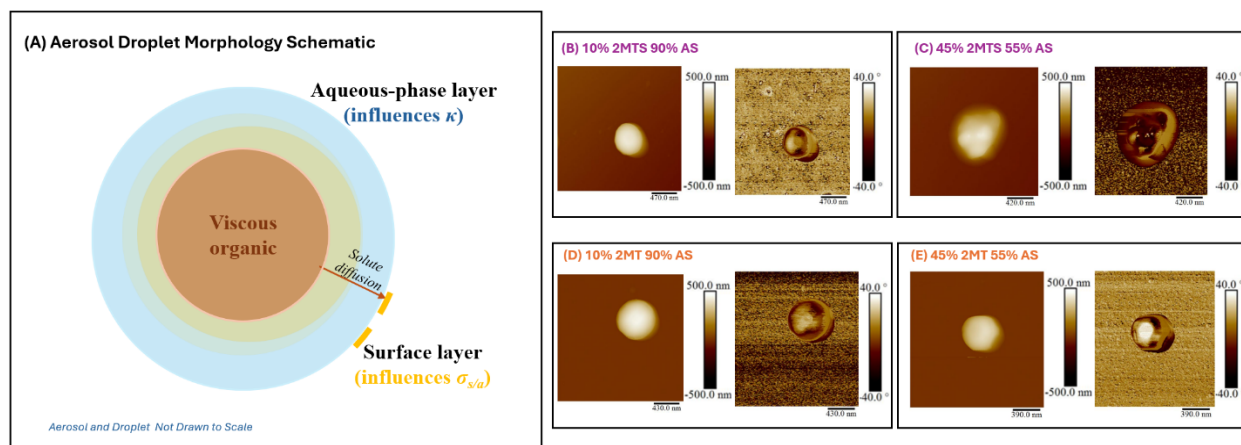


Figure 4. (A) Schematic depicting aerosol droplet composed of a viscous organic core and aqueous phase layer and AFM images of (B) 10 wt% 2-MTS – 90 wt% AS (C) 45 wt% 2-MTS – 55 wt% AS (D) 10 wt% 2-MT – 90 wt% AS and (E) 45 wt% 2-MT – 90 wt% AS. AFM results depict vertical particle height (left) and phase morphology (right).

567 roughness in the outer edge which can promote “cracking” in the organic phase, which can result
568 in full dissolution in the presence of higher water content and ideal mixing (Tandon et al., 2019).

569 As 2-MTS is increased to 45 wt%, the particle morphology shows greater inorganic phase
570 dispersion, with AS protruding through the viscous organic phase (Fig. 4C). The visualized
571 morphology and phase state of the particle agrees with behavior inferred from water-uptake and
572 droplet measurements (Sect. 4.2). In particular, ~ 45 wt% is the observed threshold for the plateau

573 in 2-MTS/AS $\kappa_{\text{H-TDMA}}$ values, prior to a linear decrease in $\kappa_{\text{H-TDMA}}$ values. The dispersion of AS
574 disrupts the organic network within the viscous phase, giving rise to the observed roughness and
575 promoting the salting in of 2-MTS. This phenomenon agrees with the results of previously
576 published literature that show viscous organics mixed with AS; specifically, laboratory-generated
577 SOA-AS and citric acid-AS mixtures (Saukko et al., 2012; Abramson et al., 2013). Previous
578 studies have also observed increased diffusion within viscous SOA particles via a disruption of the
579 hydrogen bonding network between the organic molecules that can promote solute movement in
580 the droplet (Reid et al., 2018; Jeong et al., 2022; Sheldon et al., 2023). For this reason, it is likely
581 that greater organic diffusion occurs above 45 wt% organic, resulting in decreasing $\kappa_{\text{H-TDMA}}$ values.
582 Furthermore, the well dispersed AFM morphology is indicative of ideal mixing under
583 supersaturated conditions, thereby agreeing with κ -Köhler theory of droplet growth.

584 In comparison, 2-MT mixtures present an engulfed core-shell morphology from 10 to 45 wt%
585 organic (Fig. 4D-E). At 10 wt% 2-MT, the viscous organic phase dominates the particle
586 morphology and AS remains dispersed at the surface edge, as shown in Fig. 4D. As organic wt%
587 increases to 45 wt%, morphology remains unchanged and the organic phase stays intact. The intact
588 core-shell morphology of 45 wt% 2-MT aerosol mimic contrasts with the well dispersed
589 morphology observed for 45 wt% 2-MTS aerosol mimic. For 2-MT, the organic diffusion is
590 limited under both sub- and supersaturated conditions, likely due to the undissolved viscous
591 organic phase (Fig. 4A). Specifically, 2-MT viscosity causes slower dissolution compared to AS
592 and results in the phase separated morphology. Thus, hygroscopicity of the 2-MT/AS mixture is
593 dominated by AS dissolution from the core and outer shell, corresponding to the hygroscopic
594 plateau observed for 2-MT/AS sub- and supersaturated water uptake measurements (Fig. 3).
595 Therefore, particle morphology and viscosity influence the synthesized 2-MT's ability to diffuse
596 through the aerosol droplet and can affect aerosol water uptake process. Indeed, a previous study
597 by Zhang et al. (2018) described the self-limiting effect of a core-shell morphology on IEPOX-
598 SOA reactive uptake and can now be observed in the 2-MT/AS water uptake process. However,
599 diffusion limitations can also result in the need for longer time periods to reach an equilibrium
600 state, as observed by dynamic surface tension measurements. Consequently, current
601 hygroscopicity measurements that occur at fast time scales may not capture the full water uptake
602 process of the synthesized organics and their mixtures. For example, the residence of aerosols
603 within DMT CCNC columns is ~ 10 s (Paramonov et al., 2015) while similar H-TDMA instrument
604 set ups have a residence time ~ 6.5 s (Mikhailov & Vlasenko, 2020). However, a previous study
605 by Chuang et al. (2003) found atmospheric droplet growth timescales range between 5 to 100 s,
606 congruent with the timescale of 2-MT and 2-MTS dynamic surface tension change (Fig. 2. and
607 Chuang, 2003). Therefore, hygroscopicity of viscous organic containing aerosols, such as 2-MT
608 and 2-MTS, must be studied at greater residence times to observe any possible effects on
609 hygroscopicity; understanding whether timescale effects CCN activity of organic-inorganic
610 aerosol mixtures can greatly impact current global models that may assume instantaneous solute
611 dissolution during the water uptake process. Furthermore, future studies should consider whether
612 the hygroscopicity approximations of viscous 2-MT/AS and 2-MTS/AS mixtures are time
613 dependent, as time-dependent droplet formation has been observed for biogenic aerosols (Vizenor
614 & Asa-Awuku, 2018). Currently, traditional κ -Köhler theory is unable to predict the water uptake
615 of 2-MT/AS and subsaturated 2-MTS/AS aerosols and does not consider solute and droplet kinetic

616 effects. However, by accounting for phase morphology and viscosity, κ predictions may be
617 improved.

618 In addition, size-dependent morphology may also affect κ -hygroscopicity estimations. Several
619 studies observe a relationship between particle size and aerosol phase transitions during water
620 uptake (Veghte et al., 2013; Cheng et al., 2015; Altaf et al., 2016; Schmedding & Zuend, 2025).
621 Specifically, Veghte et al. (2013) and Cheng et al. (2015) observe smaller AS-organic particles
622 favoring a homogeneous liquid phase while larger particles remain in a partially engulfed
623 morphology; this finding correlates with 2-MT/AS engulfed morphology for particles imaged \geq
624 390 nm (Fig. 4). Indeed, for 2-MT/AS mixtures > 60 wt% 2-MT, κ_{CCN} decreases with increasing
625 dry activation diameter before plateauing (Fig. S5). This trend may correlate to greater organic
626 diffusion as particle size and morphology changing before a dissolution limit is reached for > 60
627 wt% 2-MT/AS mixtures. For mixtures ≤ 60 wt% 2-MT, a similar decrease in κ_{CCN} is observed
628 before hygroscopicity begins to increase; this may be attributed to the engulfed morphology in
629 larger particles (Fig. 4D-E) promoting AS dissolution and water uptake contribution while 2-MT
630 diffusion reaches a limit. However, the water uptake measurements performed in this study do not
631 account for size-dependent phase morphology in its analysis. Therefore, future work may build
632 upon the results of this study to better parameterize hygroscopicity based on initial particle size
633 and size-dependent phase morphology affecting κ -hygroscopicity estimations. In particular, size-
634 selected CCN measurements can be performed to better probe size-dependent morphology effects
635 on aerosol activation. By doing so, global models can incorporate these influential
636 physicochemical properties into predictions of aerosol-cloud interactions.

637 5. Summary and Implications

638 In this study, we investigated the influence of solute diffusivity and droplet phase morphology on
639 the hygroscopicity of synthesized 2-MT sample, 2-MTS sample, and their mixtures with AS.
640 Mixtures with AS were varied by organic wt%. Both 2-MT and 2-MTS were previously observed
641 to be viscous and glassy, affecting diffusivity through water. Additionally, previous studies found
642 2-MT to be weakly surface-active. To determine organic diffusivity and potential surface activity,
643 dynamic surface tension measurements were taken for aqueous organic and mixed organic-
644 inorganic solutions. 2-MT and 2-MTS were found to be weakly surface-active. Previous studies
645 by Bain et al., 2023 and Mikhailov et al., 2024 determined that surface activity in the dilute bulk
646 concentration range correlates with depressed aerosol surface tension. However, neither 2-MT
647 sample nor 2-MTS sample are sufficiently surface-active to depress droplet surface tension at the
648 air-surface interface. 2-MT and 2-MTS sample solutes move slowly in droplets and have estimated
649 diffusion rates (D_s) between 10^{-9} to 10^{-11} $\text{m}^2 \text{s}^{-1}$, with diffusion slowing as organic concentration is
650 increased. When mixed with AS, 2-MT diffusivity remains slow (10^{-10} $\text{m}^2 \text{s}^{-1}$) while 2-MTS
651 diffusivity increases by an order of magnitude (10^{-9} $\text{m}^2 \text{s}^{-1}$); 2-MTS diffusion in aqueous AS-
652 mixtures is similar to other quickly dissolving compounds, such as NaCl ($D_s = 10^{-9}$, Vitagliano &
653 Lyons, 1956; Leaist & Hao, 1992) and can result in a well-mixed droplet.

654 Organic viscosity and diffusion affect aerosol water uptake (Asa-Awuku & Nenes, 2007; Bones et
655 al., 2012; Tandon et al., 2019). For 2-MT, 2-MTS sample, and subsequent mixtures under both
656 sub- and supersaturated conditions, droplet growth is affected by solute diffusion. Subsaturated

657 droplet growth was measured using a H-TDMA at 88.2% RH and subsaturated hygroscopicity was
658 parameterized by $\kappa_{\text{H-TDMA}}$. For supersaturated conditions, a CCNC determined the activation ratio
659 of particles at varied supersaturations (0.3-1.4% SS) and water uptake was parameterized by κ_{CCN} .
660 2-MT/AS mixtures exhibit plateaued $\kappa_{\text{H-TDMA}}$ and κ_{CCN} values close to κ_{int} of AS (~0.61). A similar
661 plateau behavior is observed for 2-MTS/AS $\kappa_{\text{H-TDMA}}$. However, for supersaturated conditions, 2-
662 MTS/AS mixture κ_{CCN} follows ideal mixing behavior, represented by its proximity to κ -
663 hygroscopicity predicted by κ -Köhler theory and volume additive ZSR. Additionally, $\kappa_{\text{H-TDMA}}$
664 remains higher than κ_{CCN} ; this is a result of increased water content reducing viscosity effects and
665 enhancing organic dissolution under supersaturated conditions.

666 The κ -hygroscopicity plateau in Fig. 3 has been previously attributed to the presence of phase
667 separation, resulting in the inorganic, more soluble, and ideal compound (AS) driving water uptake
668 (Malek et al., 2023). However, for 2-MTS /AS ideal hygroscopic behavior is indicative of a well
669 dissolved, homogeneous droplet (Petters & Kreidenweis, 2007). To better understand phase
670 morphology of the synthesized organic-AS mixed particles, AFM measurements of synthesized 2-
671 MTS, 2-MTS/AS mixtures, and 2-MT/AS mixtures were acquired. 2-MTS aerosols are smooth,
672 spherical, viscous particles; when mixed with AS at 10 wt%, AS remains in the aqueous core and
673 is dispersed on the side of the particle, introducing roughness on the aerosol outer shell. As organic
674 concentration increases, the AS core is broken up through the particle. The less defined core-shell
675 morphology may be the result of AS disrupting the interactions between neighboring 2-MTS
676 particles in the viscous network; as a result, organic dissolution becomes faster as indicated by
677 greater 2-MTS diffusion rates. Thus, 2-MTS sample/AS aerosols behave similar to traditional full
678 dissolution assumptions. In comparison, 2-MT/AS mixture AFM images show an engulfed core-
679 shell morphology regardless of organic concentration. As a result, the viscous organic phase
680 remains intact while aqueous AS in the core drives hygroscopicity. A caveat to these results is the
681 presence of SMS, an organosulfate, being present within the 2-MTS sample at ~24 wt%. Therefore,
682 SMS may have an effect on surface tension, diffusivity, and hygroscopic trends observed for the
683 2-MTS sample/AS mixtures that is currently unknown in this study. Future work may utilize the
684 methodology laid out in this work to more deeply probe the influence of SMS and any additional
685 mixture component on viscous organic properties and water uptake.

686 This study demonstrates that viscosity can dictate organic diffusion through aqueous droplets,
687 resulting in complex phase morphology and water uptake properties. Furthermore, the synthesized
688 samples studied in this work a representative of the hygroscopic properties of IEPOX-SOA
689 mixtures. A recent study by Armstrong et al. (2025) determined that the IEPOX-SOA composition
690 is composed of a range of 2-MT, 2-MTS, and additional components that vary with aerosol acidity.
691 Thus, the synthesized samples present in this work may present a subset of SOA aerosols generated
692 and this study provides insight into its potential diffusive, hygroscopic, and phase behavior. For
693 example, as shown by this study's water uptake measurements, hygroscopicity from the
694 subsaturated to supersaturated regime evolves due to the presence of increased water content.
695 However, it is also noted that the hygroscopicity measurements performed in this study were on
696 short time scales (6-10 s); in comparison, dynamic surface tension measurements showed droplet
697 equilibrium being reached at 100-300 s for aqueous 2-MT, 2-MT/AS, and 2-MTS. Thus, current
698 water uptake measurements may not capture a potentially evolving hygroscopicity over time. This

699 is critical in understanding biogenic aerosol influence on cloud formation; a previous study by
700 Chuang (2003) found that droplet formation can occur within time scales of 5-100 s, well within
701 evolving diffusion times observed in this study. Therefore, future work must investigate potentially
702 dynamic water uptake of viscous biogenic aerosols, such as 2-MT, 2-MTS. Furthermore, time
703 dependent κ can be developed to better account for organic diffusion within larger scale cloud
704 parcel and global models. In addition to time dependency, κ -hygroscopicity estimations may also
705 be affected by size dependent phase morphology. A study by Veghte et al. (2013) found smaller
706 aerosol particles preferring a homogenous state, while larger particles have an engulfed core-shell
707 morphology similar to 2-MT/AS aerosols in this study. Therefore, particle size may influence
708 viscous organic-AS water uptake due to diffusion and morphological influences. Future work may
709 explore and parameterize the effect of size-dependent phase separated morphology on aerosol
710 activation through step size-selected CCN measurements. Ultimately, it is crucial to understand
711 how biogenic aerosols, such as 2-MT and 2-MTS, properties (viscosity, diffusivity, and phase
712 morphology) alter cloud formation. The results of this study demonstrate the co-dependency of
713 these properties for two isoprene derived compounds and thus may improve our overall
714 understanding of how biogenic aerosols, and their mixtures affect aerosol-cloud interactions.

715 **Author Contributions:** NF designed, collected, analyzed all experimental data, and analyzed
716 theoretical models. CA contributed to design and analysis of water uptake data. SJ contributed to
717 design and collection of H-TDMA experimental data. AD contributed to design and analysis of
718 AFM data. MA contributed to design and collection of AFM data. ERR contributed to collection
719 of surface tension experimental data. ZZ and AG contributed to sample synthesis. JLW contributed
720 to design, collection, and analysis of dynamic surface tension experimental data. YZ contributed
721 to viscosity, diffusion, and AFM data analysis. All authors contributed to the writing and
722 preparation of the manuscript.

723 **Competing Interest Statement:** The authors have no competing interests to declare

724

725 **Acknowledgements:**

726 The authors acknowledge the support of this work by NSF under AGS #2131369, AGS #2124489,
727 AGS #2131369 (Y.Z.), AGS #2131370 (J.S.), and AGS #2304669 (A.G., Z.Z., J.D.S.).

728 The authors acknowledge the characterization part of this work was performed in Texas A&M
729 University Materials Characterization Core Facility (RRID:SCR_022202).

730

731

732

733

734 Abramson, E., Imre, D., Beránek, J., Wilson, J., & Zelenyuk, A. (2013). Experimental determination of
735 chemical diffusion within secondary organic aerosol particles [10.1039/C2CP44013J].

736 *Physical Chemistry Chemical Physics*, 15(8), 2983–2991.
737 <https://doi.org/10.1039/C2CP44013J>

738 Albrecht, B. A. (1989). Aerosols, Cloud Microphysics, and Fractional Cloudiness. *Science*,
739 245(4923), 1227–1230. <https://doi.org/doi:10.1126/science.245.4923.1227>

740 Altaf, M. B., Zuend, A., & Freedman, M. A. (2016). Role of nucleation mechanism on the size
741 dependent morphology of organic aerosol [10.1039/C6CC03826C]. *Chemical*
742 *Communications*, 52(59), 9220–9223. <https://doi.org/10.1039/C6CC03826C>

743 Armstrong, N. C., Gagan, S., Doderio, A. J., Ferdousi-Rokib, N., Frauenheim, M., Gold, A., Zhang, Z.,
744 Asa-Awuku, A., Zhang, Y., & Surratt, J. D. (2025). Hygroscopicity Depends on Aerosol Acidity
745 and Sulfate Content during the Reactive Uptake of Isoprene Epoxydiols. *ACS Earth and*
746 *Space Chemistry*. <https://doi.org/10.1021/acsearthspacechem.5c00163>

747 Asa-Awuku, A., & Nenes, A. (2007). Effect of solute dissolution kinetics on cloud droplet formation:
748 Extended Köhler theory. *Journal of Geophysical Research: Atmospheres*, 112(D22).
749 <https://doi.org/https://doi.org/10.1029/2005JD006934>

750 Bain, A., Ghosh, K., Prisle, N. L., & Bzdek, B. R. (2023). Surface-Area-to-Volume Ratio Determines
751 Surface Tensions in Microscopic, Surfactant-Containing Droplets. *ACS Central Science*,
752 9(11), 2076–2083. <https://doi.org/10.1021/acscentsci.3c00998>

753 Bain, A., Lalemi, L., Croll Dawes, N., Miles, R. E. H., Prophet, A. M., Wilson, K. R., & Bzdek, B. R.
754 (2024). Surfactant Partitioning Dynamics in Freshly Generated Aerosol Droplets. *Journal of*
755 *the American Chemical Society*, 146(23), 16028–16038.
756 <https://doi.org/10.1021/jacs.4c03041>

757 Beier, T., Cotter, E. R., Galloway, M. M., & Woo, J. L. (2019). In Situ Surface Tension Measurements
758 of Hanging Droplet Methylglyoxal/Ammonium Sulfate Aerosol Mimics under Photooxidative
759 Conditions. *ACS Earth and Space Chemistry*, 3(7), 1208–1215.
760 <https://doi.org/10.1021/acsearthspacechem.9b00123>

761 Bertram, A. K., Martin, S. T., Hanna, S. J., Smith, M. L., Bodsworth, A., Chen, Q., Kuwata, M., Liu, A.,
762 You, Y., & Zorn, S. R. (2011). Predicting the relative humidities of liquid-liquid phase
763 separation, efflorescence, and deliquescence of mixed particles of ammonium sulfate,
764 organic material, and water using the organic-to-sulfate mass ratio of the particle and the
765 oxygen-to-carbon elemental ratio of the organic component. *Atmos. Chem. Phys.*, 11(21),
766 10995–11006. <https://doi.org/10.5194/acp-11-10995-2011>

767 Bondy, A. L., Bonanno, D., Moffet, R. C., Wang, B., Laskin, A., & Ault, A. P. (2018). The diverse
768 chemical mixing state of aerosol particles in the southeastern United States. *Atmos. Chem.*
769 *Phys.*, 18(16), 12595–12612. <https://doi.org/10.5194/acp-18-12595-2018>

770 Bones, D. L., Reid, J. P., Lienhard, D. M., & Krieger, U. K. (2012). Comparing the mechanism of water
771 condensation and evaporation in glassy aerosol. *Proceedings of the National Academy of*
772 *Sciences*, 109(29), 11613–11618. <https://doi.org/doi:10.1073/pnas.1200691109>

773 Chan, M. N., Surratt, J. D., Claeys, M., Edgerton, E. S., Tanner, R. L., Shaw, S. L., Zheng, M., Knipping,
774 E. M., Eddingsaas, N. C., Wennberg, P. O., & Seinfeld, J. H. (2010). Characterization and
775 Quantification of Isoprene-Derived Epoxydiols in Ambient Aerosol in the Southeastern
776 United States. *Environmental Science & Technology*, 44(12), 4590–4596.
777 <https://doi.org/10.1021/es100596b>

778 Chen, B., Mirrielees, J. A., Chen, Y., Onasch, T. B., Zhang, Z., Gold, A., Surratt, J. D., Zhang, Y., &
779 Brooks, S. D. (2023). Glass Transition Temperatures of Organic Mixtures from Isoprene
780 Epoxydiol-Derived Secondary Organic Aerosol. *The Journal of Physical Chemistry A*, 127(18),
781 4125–4136. <https://doi.org/10.1021/acs.jpca.2c08936>

782 Chen, Y., Dombek, T., Hand, J., Zhang, Z., Gold, A., Ault, A. P., Levine, K. E., & Surratt, J. D. (2021).
783 Seasonal Contribution of Isoprene-Derived Organosulfates to Total Water-Soluble Fine

784 Particulate Organic Sulfur in the United States. *ACS Earth and Space Chemistry*, 5(9), 2419–
785 2432. <https://doi.org/10.1021/acsearthspacechem.1c00102>

786 Cheng, Y., Su, H., Koop, T., Mikhailov, E., & Pöschl, U. (2015). Size dependence of phase transitions
787 in aerosol nanoparticles. *Nature Communications*, 6(1), 5923.
788 <https://doi.org/10.1038/ncomms6923>

789 Chenyakin, Y., Ullmann, D. A., Evoy, E., Renbaum-Wolff, L., Kamal, S., & Bertram, A. K. (2017).
790 Diffusion coefficients of organic molecules in sucrose–water solutions and comparison with
791 Stokes–Einstein predictions. *Atmos. Chem. Phys.*, 17(3), 2423–2435.
792 <https://doi.org/10.5194/acp-17-2423-2017>

793 Chernyshev, V. S., & Skliar, M. (2015). Diffusivity Measurements of Solutes Impacting Interfacial
794 Tension. *Industrial & Engineering Chemistry Research*, 54(16), 4535–4544.
795 <https://doi.org/10.1021/ie504355w>

796 Chuang, P. Y. (2003). Measurement of the timescale of hygroscopic growth for atmospheric
797 aerosols. *Journal of Geophysical Research: Atmospheres*, 108(D9).
798 <https://doi.org/https://doi.org/10.1029/2002JD002757>

799 Claeys, M., Graham, B., Vas, G., Wang, W., Vermeylen, R., Pashynska, V., Cafmeyer, J., Guyon, P.,
800 Andreae, M. O., Artaxo, P., & Maenhaut, W. (2004). Formation of Secondary Organic Aerosols
801 Through Photooxidation of Isoprene. *Science*, 303(5661), 1173–1176.
802 <https://doi.org/doi:10.1126/science.1092805>

803 Cooke, M. E., Armstrong, N. C., Lei, Z., Chen, Y., Waters, C. M., Zhang, Y., Buchenau, N. A., Dibley,
804 M. Q., Ledsky, I. R., Szalkowski, T., Lee, J. Y., Baumann, K., Zhang, Z., Vizuete, W., Gold, A.,
805 Surratt, J. D., & Ault, A. P. (2022). Organosulfate Formation in Proxies for Aged Sea Spray
806 Aerosol: Reactive Uptake of Isoprene Epoxydiols to Acidic Sodium Sulfate. *ACS Earth and*
807 *Space Chemistry*, 6(12), 2790–2800. <https://doi.org/10.1021/acsearthspacechem.2c00156>

808 Curry, L. A., Tsui, W. G., & McNeill, V. F. (2018). Technical note: Updated parameterization of the
809 reactive uptake of glyoxal and methylglyoxal by atmospheric aerosols and cloud droplets.
810 *Atmos. Chem. Phys.*, 18(13), 9823–9830. <https://doi.org/10.5194/acp-18-9823-2018>

811 Cziczo, D. J., Nowak, J. B., Hu, J. H., & Abbatt, J. P. D. (1997). Infrared spectroscopy of model
812 tropospheric aerosols as a function of relative humidity: Observation of deliquescence and
813 crystallization. *Journal of Geophysical Research: Atmospheres*, 102(D15), 18843–18850.
814 <https://doi.org/https://doi.org/10.1029/97JD01361>

815 DeCarlo, P. F., Slowik, J. G., Worsnop, D. R., Davidovits, P., & Jimenez, J. L. (2004). Particle
816 Morphology and Density Characterization by Combined Mobility and Aerodynamic Diameter
817 Measurements. Part 1: Theory. *Aerosol Science and Technology*, 38(12), 1185–1205.
818 <https://doi.org/10.1080/027868290903907>

819 DeRieux, W. S. W., Li, Y., Lin, P., Laskin, J., Laskin, A., Bertram, A. K., Nizkorodov, S. A., & Shiraiwa,
820 M. (2018). Predicting the glass transition temperature and viscosity of secondary organic
821 material using molecular composition. *Atmos. Chem. Phys.*, 18(9), 6331–6351.
822 <https://doi.org/10.5194/acp-18-6331-2018>

823 Eastoe, J., Dalton, J. S., Rogueda, P. G. A., & Griffiths, P. C. (1998). Evidence for Activation–Diffusion
824 Controlled Dynamic Surface Tension with a Nonionic Surfactant. *Langmuir*, 14(5), 979–981.
825 <https://doi.org/10.1021/la971241w>

826 Einstein, A. (1905). Über die von der molekularkinetischen Theorie der Wärme geforderte Bewegung
827 von in ruhenden Flüssigkeiten suspendierten Teilchen. *Annalen der Physik*, 322(8), 549–560.
828 <https://doi.org/https://doi.org/10.1002/andp.19053220806>

829 El Haber, M., Ferronato, C., Giroir-Fendler, A., Fine, L., & Nozière, B. (2023). Salting out, non-ideality
830 and synergism enhance surfactant efficiency in atmospheric aerosols. *Scientific Reports*,
831 13(1), 20672. <https://doi.org/10.1038/s41598-023-48040-5>

832 Ferdousi-Rokib, N., A. Malek, K., Mitchell, I., M. Fierce, L., & Asa-Awuku, A. A. (2025). Aerosol
833 Hygroscopicity and Surface-Active Coverage for the Droplet Growth of Aerosol Mixtures. *ACS*
834 *ES&T Air*, 2(8), 1454–1467. <https://doi.org/10.1021/acsestair.4c00303>

835 Fertil, D., Pierre-Louis, K., Ingwer, S., Galloway, M. M., & Woo, J. L. (2025). Surfactant Effects in
836 Irradiated, Hanging-Droplet, Aqueous-Phase Glyoxal/Ammonium Sulfate Aerosol Mimic
837 Systems. *ACS Earth and Space Chemistry*.
838 <https://doi.org/10.1021/acsearthspacechem.4c00288>

839 Fordham, S., & Freeth, F. A. (1948). On the calculation of surface tension from measurements of
840 pendant drops. *Proceedings of the Royal Society of London. Series A. Mathematical and*
841 *Physical Sciences*, 194(1036), 1–16. <https://doi.org/doi:10.1098/rspa.1948.0063>

842 Freedman, M. A. (2017). Phase separation in organic aerosol [10.1039/C6CS00783J]. *Chemical*
843 *Society Reviews*, 46(24), 7694–7705. <https://doi.org/10.1039/C6CS00783J>

844 Froyd, K. D., Murphy, S. M., Murphy, D. M., de Gouw, J. A., Eddingsaas, N. C., & Wennberg, P. O.
845 (2010). Contribution of isoprene-derived organosulfates to free tropospheric aerosol mass.
846 *Proceedings of the National Academy of Sciences*, 107(50), 21360–21365.
847 <https://doi.org/doi:10.1073/pnas.1012561107>

848 Fuchs, N. A. (1963). On the stationary charge distribution on aerosol particles in a bipolar ionic
849 atmosphere. *Geofisica pura e applicata*, 56(1), 185–193.
850 <https://doi.org/10.1007/BF01993343>

851 Gohil, K. (2022). *kgohil27/PyCAT: v1.0 (v1.0)*. Zenodo.

852 Gohil, K., & Asa-Awuku, A. A. (2022). Cloud condensation nuclei (CCN) activity analysis of low-
853 hygroscopicity aerosols using the aerodynamic aerosol classifier (AAC). *Atmos. Meas. Tech.*,
854 15(4), 1007–1019. <https://doi.org/10.5194/amt-15-1007-2022>

855 Guenther, A. B., Jiang, X., Heald, C. L., Sakulyanontvittaya, T., Duhl, T., Emmons, L. K., & Wang, X.
856 (2012). The Model of Emissions of Gases and Aerosols from Nature version 2.1 (MEGAN2.1):
857 an extended and updated framework for modeling biogenic emissions. *Geosci. Model Dev.*,
858 5(6), 1471–1492. <https://doi.org/10.5194/gmd-5-1471-2012>

859 Hettiyadura, A. P. S., Al-Naiema, I. M., Hughes, D. D., Fang, T., & Stone, E. A. (2019). Organosulfates
860 in Atlanta, Georgia: anthropogenic influences on biogenic secondary organic aerosol
861 formation. *Atmos. Chem. Phys.*, 19(5), 3191–3206. [https://doi.org/10.5194/acp-19-3191-](https://doi.org/10.5194/acp-19-3191-2019)
862 [2019](https://doi.org/10.5194/acp-19-3191-2019)

863 Hughes, D. D., Christiansen, M. B., Milani, A., Vermeuel, M. P., Novak, G. A., Alwe, H. D., Dickens, A.
864 F., Pierce, R. B., Millet, D. B., Bertram, T. H., Stanier, C. O., & Stone, E. A. (2021). PM_{2.5}
865 chemistry, organosulfates, and secondary organic aerosol during the 2017 Lake Michigan
866 Ozone Study. *Atmospheric Environment*, 244, 117939.
867 <https://doi.org/https://doi.org/10.1016/j.atmosenv.2020.117939>

868 Hyvärinen, A.-P., Raatikainen, T., Laaksonen, A., Viisanen, Y., & Lihavainen, H. (2005). Surface
869 tensions and densities of H₂SO₄ + NH₃ + water solutions. *Geophysical Research Letters*,
870 32(16). <https://doi.org/https://doi.org/10.1029/2005GL023268>

871 Intergovernmental Panel on Climate, C. (2023). *Climate Change 2021 – The Physical Science Basis:*
872 *Working Group I Contribution to the Sixth Assessment Report of the Intergovernmental Panel*
873 *on Climate Change*. Cambridge University Press. [https://doi.org/DOI:](https://doi.org/DOI:10.1017/9781009157896)
874 [10.1017/9781009157896](https://doi.org/DOI:10.1017/9781009157896)

875 Jeong, R., Lilek, J., Zuend, A., Xu, R., Chan, M. N., Kim, D., Moon, H. G., & Song, M. (2022). Viscosity
876 and physical state of sucrose mixed with ammonium sulfate droplets. *Atmos. Chem. Phys.*,
877 22(13), 8805–8817. <https://doi.org/10.5194/acp-22-8805-2022>

878 Joos, P., & Rillaerts, E. (1981). Theory on the determination of the dynamic surface tension with the
879 drop volume and maximum bubble pressure methods. *Journal of Colloid and Interface*
880 *Science*, 79(1), 96–100. [https://doi.org/https://doi.org/10.1016/0021-9797\(81\)90051-5](https://doi.org/https://doi.org/10.1016/0021-9797(81)90051-5)

881 Kampf, C. J., Waxman, E. M., Slowik, J. G., Dommen, J., Pfaffenberger, L., Praplan, A. P., Prévôt, A. S.
882 H., Baltensperger, U., Hoffmann, T., & Volkamer, R. (2013). Effective Henry's Law Partitioning
883 and the Salting Constant of Glyoxal in Aerosols Containing Sulfate. *Environmental Science &*
884 *Technology*, 47(9), 4236–4244. <https://doi.org/10.1021/es400083d>

885 Kanakidou, M., Seinfeld, J. H., Pandis, S. N., Barnes, I., Dentener, F. J., Facchini, M. C., Van Dingenen,
886 R., Ervens, B., Nenes, A., Nielsen, C. J., Swietlicki, E., Putaud, J. P., Balkanski, Y., Fuzzi, S.,
887 Horth, J., Moortgat, G. K., Winterhalter, R., Myhre, C. E. L., Tsigaridis, K., . . . Wilson, J. (2005).
888 Organic aerosol and global climate modelling: a review. *Atmos. Chem. Phys.*, 5(4), 1053–
889 1123. <https://doi.org/10.5194/acp-5-1053-2005>

890 Kang, B., Tang, H., Zhao, Z., & Song, S. (2020). Hofmeister Series: Insights of Ion Specificity from
891 Amphiphilic Assembly and Interface Property. *ACS Omega*, 5(12), 6229–6239.
892 <https://doi.org/10.1021/acsomega.0c00237>

893 Kleinheins, J., Shardt, N., Lohmann, U., & Marcolli, C. (2025). The surface tension and cloud
894 condensation nuclei (CCN) activation of sea spray aerosol particles. *Atmos. Chem. Phys.*,
895 25(2), 881–903. <https://doi.org/10.5194/acp-25-881-2025>

896 Köhler, H. (1936). The nucleus in and the growth of hygroscopic droplets [10.1039/TF9363201152].
897 *Transactions of the Faraday Society*, 32(0), 1152–1161.
898 <https://doi.org/10.1039/TF9363201152>

899 Kreidenweis, S. M., & Asa-Awuku, A. (2014). 5.13 - Aerosol Hygroscopicity: Particle Water Content
900 and Its Role in Atmospheric Processes. In H. D. Holland & K. K. Turekian (Eds.), *Treatise on*
901 *Geochemistry (Second Edition)* (pp. 331–361). Elsevier.
902 <https://doi.org/https://doi.org/10.1016/B978-0-08-095975-7.00418-6>

903 Lance, S., Nenes, A., Medina, J., & Smith, J. N. (2006). Mapping the Operation of the DMT Continuous
904 Flow CCN Counter. *Aerosol Science and Technology*, 40(4), 242–254.
905 <https://doi.org/10.1080/02786820500543290>

906 Laskina, O., Morris, H. S., Grandquist, J. R., Qin, Z., Stone, E. A., Tivanski, A. V., & Grassian, V. H.
907 (2015). Size Matters in the Water Uptake and Hygroscopic Growth of Atmospherically
908 Relevant Multicomponent Aerosol Particles. *The Journal of Physical Chemistry A*, 119(19),
909 4489–4497. <https://doi.org/10.1021/jp510268p>

910 Leaist, D. G., & Hao, L. (1992). Binary mutual diffusion coefficients of aqueous ammonium and
911 potassium sulfates at 25°C. *Journal of Solution Chemistry*, 21(4), 345–350.
912 <https://doi.org/10.1007/BF00647857>

913 Malek, K., Gohil, K., Olonimoyo, E. A., Ferdousi-Rokib, N., Huang, Q., Pitta, K. R., Nandy, L., Voss, K.
914 A., Raymond, T. M., Dutcher, D. D., Freedman, M. A., & Asa-Awuku, A. (2023). Liquid–Liquid
915 Phase Separation Can Drive Aerosol Droplet Growth in Supersaturated Regimes. *ACS*
916 *Environmental Au*. <https://doi.org/10.1021/acsenvironau.3c00015>

917 Mikhailov, E. F., & Vlasenko, S. S. (2020). High-humidity tandem differential mobility analyzer for
918 accurate determination of aerosol hygroscopic growth, microstructure, and activity
919 coefficients over a wide range of relative humidity. *Atmos. Meas. Tech.*, 13(4), 2035–2056.
920 <https://doi.org/10.5194/amt-13-2035-2020>

921 Mikhailov, E. F., Vlasenko, S. S., & Kiselev, A. A. (2024). Water activity and surface tension of aqueous
922 ammonium sulfate and D-glucose aerosol nanoparticles. *Atmos. Chem. Phys.*, 24(5), 2971–
923 2984. <https://doi.org/10.5194/acp-24-2971-2024>

924 Moore, R. H., Nenes, A., & Medina, J. (2010). Scanning Mobility CCN Analysis—A Method for Fast
925 Measurements of Size-Resolved CCN Distributions and Activation Kinetics. *Aerosol Science*
926 *and Technology*, 44(10), 861–871. <https://doi.org/10.1080/02786826.2010.498715>

927 Murphy, D. M., Thomson, D. S., & Mahoney, M. J. (1998). In Situ Measurements of Organics,
928 Meteoritic Material, Mercury, and Other Elements in Aerosols at 5 to 19 Kilometers. *Science*,
929 282(5394), 1664–1669. <https://doi.org/doi:10.1126/science.282.5394.1664>

930 O'Meara, S., Topping, D. O., & McFiggans, G. (2016). The rate of equilibration of viscous aerosol
931 particles. *Atmos. Chem. Phys.*, 16(8), 5299–5313. [https://doi.org/10.5194/acp-16-5299-](https://doi.org/10.5194/acp-16-5299-2016)
932 [2016](https://doi.org/10.5194/acp-16-5299-2016)

933 Ott, E.-J. E., Tackman, E. C., & Freedman, M. A. (2020). Effects of Sucrose on Phase Transitions of
934 Organic/Inorganic Aerosols. *ACS Earth and Space Chemistry*, 4(4), 591–601.
935 <https://doi.org/10.1021/acsearthspacechem.0c00006>

936 Padró, L. T., Tkacik, D., Latham, T., Hennigan, C. J., Sullivan, A. P., Weber, R. J., Huey, L. G., & Nenes,
937 A. (2010). Investigation of cloud condensation nuclei properties and droplet growth kinetics
938 of the water-soluble aerosol fraction in Mexico City. *Journal of Geophysical Research:*
939 *Atmospheres*, 115(D9). <https://doi.org/https://doi.org/10.1029/2009JD013195>

940 Paramonov, M., Kerminen, V. M., Gysel, M., Aalto, P. P., Andreae, M. O., Asmi, E., Baltensperger, U.,
941 Bougiatioti, A., Brus, D., Frank, G. P., Good, N., Gunthe, S. S., Hao, L., Irwin, M., Jaatinen, A.,
942 Jurányi, Z., King, S. M., Kortelainen, A., Kristensson, A., . . . Sierau, B. (2015). A synthesis of
943 cloud condensation nuclei counter (CCNC) measurements within the EUCAARI network.
944 *Atmos. Chem. Phys.*, 15(21), 12211–12229. <https://doi.org/10.5194/acp-15-12211-2015>

945 Paulot, F., Crouse, J. D., Kjaergaard, H. G., Kürten, A., St. Clair, J. M., Seinfeld, J. H., & Wennberg, P.
946 O. (2009). Unexpected Epoxide Formation in the Gas-Phase Photooxidation of Isoprene.
947 *Science*, 325(5941), 730–733. <https://doi.org/doi:10.1126/science.1172910>

948 Peng, C., Razafindrambinina, P. N., Malek, K. A., Chen, L., Wang, W., Huang, R. J., Zhang, Y., Ding,
949 X., Ge, M., Wang, X., Asa-Awuku, A. A., & Tang, M. (2021). Interactions of organosulfates with
950 water vapor under sub- and supersaturated conditions. *Atmos. Chem. Phys.*, 21(9), 7135–
951 7148. <https://doi.org/10.5194/acp-21-7135-2021>

952 Petters, M. D., & Kreidenweis, S. M. (2007). A single parameter representation of hygroscopic growth
953 and cloud condensation nucleus activity. *Atmos. Chem. Phys.*, 7(8), 1961–1971.
954 <https://doi.org/10.5194/acp-7-1961-2007>

955 Pratt, K. A., & Prather, K. A. (2010). Aircraft measurements of vertical profiles of aerosol mixing
956 states. *Journal of Geophysical Research: Atmospheres*, 115(D11).
957 <https://doi.org/https://doi.org/10.1029/2009JD013150>

958 Prisle, N., & Mølgaard, B. (2018). Modeling CCN activity of chemically unresolved model HULIS,
959 including surface tension, non-ideality, and surface partitioning. *Atmospheric Chemistry and*
960 *Physics Discussions*, 1–23. <https://doi.org/10.5194/acp-2018-789>

961 Prisle, N. L., Engelhart, G. J., Bilde, M., & Donahue, N. M. (2010). Humidity influence on gas-particle
962 phase partitioning of α -pinene + O₃ secondary organic aerosol. *Geophysical Research*
963 *Letters*, 37(1). <https://doi.org/https://doi.org/10.1029/2009GL041402>

964 Pruppacher, H. R., Klett, J. D., & Springer. (1997). *Microphysics of Clouds and Precipitation*. Springer.
965 <https://books.google.com/books?id=Nk40jwEACAAJ>

966 Reid, J. P., Bertram, A. K., Topping, D. O., Laskin, A., Martin, S. T., Petters, M. D., Pope, F. D., & Rovelli,
967 G. (2018). The viscosity of atmospherically relevant organic particles. *Nature*
968 *Communications*, 9(1), 956. <https://doi.org/10.1038/s41467-018-03027-z>

969 Renbaum-Wolff, L., Grayson, J. W., Bateman, A. P., Kuwata, M., Sellier, M., Murray, B. J., Shilling, J.
970 E., Martin, S. T., & Bertram, A. K. (2013). Viscosity of α -pinene secondary organic material and

971 implications for particle growth and reactivity. *Proceedings of the National Academy of*
972 *Sciences*, 110(20), 8014–8019. <https://doi.org/doi:10.1073/pnas.1219548110>

973 Riemer, N., Ault, A. P., West, M., Craig, R. L., & Curtis, J. H. (2019). Aerosol Mixing State:
974 Measurements, Modeling, and Impacts. *Reviews of Geophysics*, 57(2), 187–249.
975 <https://doi.org/https://doi.org/10.1029/2018RG000615>

976 Riipinen, I., Pierce, J. R., Yli-Juuti, T., Nieminen, T., Häkkinen, S., Ehn, M., Junninen, H., Lehtipalo, K.,
977 Petäjä, T., Slowik, J., Chang, R., Shantz, N. C., Abbatt, J., Leaitch, W. R., Kerminen, V. M.,
978 Worsnop, D. R., Pandis, S. N., Donahue, N. M., & Kulmala, M. (2011). Organic condensation:
979 a vital link connecting aerosol formation to cloud condensation nuclei (CCN)
980 concentrations. *Atmos. Chem. Phys.*, 11(8), 3865–3878. [https://doi.org/10.5194/acp-11-](https://doi.org/10.5194/acp-11-3865-2011)
981 [3865-2011](https://doi.org/10.5194/acp-11-3865-2011)

982 Riva, M., Chen, Y., Zhang, Y., Lei, Z., Olson, N. E., Boyer, H. C., Narayan, S., Yee, L. D., Green, H. S.,
983 Cui, T., Zhang, Z., Baumann, K., Fort, M., Edgerton, E., Budisulistiorini, S. H., Rose, C. A.,
984 Ribeiro, I. O., e Oliveira, R. L., dos Santos, E. O., . . . Surratt, J. D. (2019). Increasing Isoprene
985 Epoxydiol-to-Inorganic Sulfate Aerosol Ratio Results in Extensive Conversion of Inorganic
986 Sulfate to Organosulfur Forms: Implications for Aerosol Physicochemical Properties.
987 *Environmental Science & Technology*, 53(15), 8682–8694.
988 <https://doi.org/10.1021/acs.est.9b01019>

989 Roberts, G. C., & Nenes, A. (2005). A Continuous-Flow Streamwise Thermal-Gradient CCN Chamber
990 for Atmospheric Measurements. *Aerosol Science and Technology*, 39(3), 206–221.
991 <https://doi.org/10.1080/027868290913988>

992 Rose, D., Gunthe, S. S., Mikhailov, E., Frank, G. P., Dusek, U., Andreae, M. O., & Pöschl, U. (2008).
993 Calibration and measurement uncertainties of a continuous-flow cloud condensation nuclei
994 counter (DMT-CCNC): CCN activation of ammonium sulfate and sodium chloride aerosol
995 particles in theory and experiment. *Atmos. Chem. Phys.*, 8(5), 1153–1179.
996 <https://doi.org/10.5194/acp-8-1153-2008>

997 Ross, S. (1945). The Change of Surface Tension with Time. I. Theories of Diffusion to the Surface.
998 *Journal of the American Chemical Society*, 67(6), 990–994.
999 <https://doi.org/10.1021/ja01222a031>

1000 Ruehl, C. R., Chuang, P. Y., Nenes, A., Cappa, C. D., Kolesar, K. R., & Goldstein, A. H. (2012). Strong
1001 evidence of surface tension reduction in microscopic aqueous droplets. *Geophysical*
1002 *Research Letters*, 39(23). <https://doi.org/https://doi.org/10.1029/2012GL053706>

1003 Ruehl, C. R., Davies, J. F., & Wilson, K. R. (2016). An interfacial mechanism for cloud droplet
1004 formation on organic aerosols. *Science*, 351(6280), 1447–1450.
1005 <https://doi.org/doi:10.1126/science.aad4889>

1006 Saukko, E., Lambe, A. T., Massoli, P., Koop, T., Wright, J. P., Croasdale, D. R., Pedernera, D. A.,
1007 Onasch, T. B., Laaksonen, A., Davidovits, P., Worsnop, D. R., & Virtanen, A. (2012). Humidity-
1008 dependent phase state of SOA particles from biogenic and anthropogenic precursors.
1009 *Atmos. Chem. Phys.*, 12(16), 7517–7529. <https://doi.org/10.5194/acp-12-7517-2012>

1010 Saxena, P., et al. (1995). Organics alter hygroscopic behavior of atmospheric particles. *Journal of*
1011 *Geophysical Research: Atmospheres*, 100(D9), 18755–18770.
1012 <https://doi.org/https://doi.org/10.1029/95JD01835>

1013 Schmedding, R., & Zuend, A. (2025). The role of interfacial tension in the size-dependent phase
1014 separation of atmospheric aerosol particles. *Atmos. Chem. Phys.*, 25(1), 327–346.
1015 <https://doi.org/10.5194/acp-25-327-2025>

1016 Seinfeld, J., & Pandis, S. (1998). *Atmospheric Chemistry and Physics: From Air Pollution to Climate*
1017 *Change*.

1018 Seinfeld, J. H. (2003). TROPOSPHERIC CHEMISTRY AND COMPOSITION | Aerosols/Particles. In J. R.
1019 Holton (Ed.), *Encyclopedia of Atmospheric Sciences* (pp. 2349–2354). Academic Press.
1020 <https://doi.org/https://doi.org/10.1016/B0-12-227090-8/00438-3>

1021 Sheldon, C. S., Choczynski, J. M., Morton, K., Palacios Diaz, T., Davis, R. D., & Davies, J. F. (2023).
1022 Exploring the hygroscopicity, water diffusivity, and viscosity of organic–inorganic aerosols –
1023 a case study on internally-mixed citric acid and ammonium sulfate particles
1024 [10.1039/D2EA00116K]. *Environmental Science: Atmospheres*, 3(1), 24–34.
1025 <https://doi.org/10.1039/D2EA00116K>

1026 Shiraiwa, M., Li, Y., Tsimpidi, A. P., Karydis, V. A., Berkemeier, T., Pandis, S. N., Lelieveld, J., Koop, T.,
1027 & Pöschl, U. (2017). Global distribution of particle phase state in atmospheric secondary
1028 organic aerosols. *Nature Communications*, 8(1), 15002.
1029 <https://doi.org/10.1038/ncomms15002>

1030 Shiraiwa, M., & Seinfeld, J. H. (2012). Equilibration timescale of atmospheric secondary organic
1031 aerosol partitioning. *Geophysical Research Letters*, 39(24).
1032 <https://doi.org/https://doi.org/10.1029/2012GL054008>

1033 Sindelarova, K., Granier, C., Bouarar, I., Guenther, A., Tilmes, S., Stavrou, T., Müller, J. F., Kuhn,
1034 U., Stefani, P., & Knorr, W. (2014). Global data set of biogenic VOC emissions calculated by
1035 the MEGAN model over the last 30 years. *Atmos. Chem. Phys.*, 14(17), 9317–9341.
1036 <https://doi.org/10.5194/acp-14-9317-2014>

1037 Song, M., Marcolli, C., Krieger, U. K., Lienhard, D. M., & Peter, T. (2013). Morphologies of mixed
1038 organic/inorganic/aqueous aerosol droplets [10.1039/C3FD00049D]. *Faraday Discussions*,
1039 165(0), 289–316. <https://doi.org/10.1039/C3FD00049D>

1040 Spelt, J. (1996). *Applied Surface Thermodynamics*. Crc Press.

1041 Srivastava, D., Vu, T. V., Tong, S., Shi, Z., & Harrison, R. M. (2022). Formation of secondary organic
1042 aerosols from anthropogenic precursors in laboratory studies. *npj Climate and Atmospheric
1043 Science*, 5(1), 22. <https://doi.org/10.1038/s41612-022-00238-6>

1044 Sullivan, R. C., Moore, M. J. K., Petters, M. D., Kreidenweis, S. M., Roberts, G. C., & Prather, K. A.
1045 (2009). Effect of chemical mixing state on the hygroscopicity and cloud nucleation properties
1046 of calcium mineral dust particles. *Atmos. Chem. Phys.*, 9(10), 3303–3316.
1047 <https://doi.org/10.5194/acp-9-3303-2009>

1048 Tandon, A., Rothfuss, N. E., & Petters, M. D. (2019). The effect of hydrophobic glassy organic material
1049 on the cloud condensation nuclei activity of particles with different morphologies. *Atmos.
1050 Chem. Phys.*, 19(5), 3325–3339. <https://doi.org/10.5194/acp-19-3325-2019>

1051 Toivola, M., Prisle, N. L., Elm, J., Waxman, E. M., Volkamer, R., & Kurtén, T. (2017). Can COSMOTherm
1052 Predict a Salting in Effect? *The Journal of Physical Chemistry A*, 121(33), 6288–6295.
1053 <https://doi.org/10.1021/acs.jpca.7b04847>

1054 Topping, D. (2010). An analytical solution to calculate bulk mole fractions for any number of
1055 components in aerosol droplets after considering partitioning to a surface layer. *Geosci.
1056 Model Dev.*, 3(2), 635–642. <https://doi.org/10.5194/gmd-3-635-2010>

1057 Topping, D. O., McFiggans, G. B., Kiss, G., Varga, Z., Facchini, M. C., Decesari, S., & Mircea, M. (2007).
1058 Surface tensions of multi-component mixed inorganic/organic aqueous systems of
1059 atmospheric significance: measurements, model predictions and importance for cloud
1060 activation predictions. *Atmos. Chem. Phys.*, 7(9), 2371–2398. <https://doi.org/10.5194/acp-7-2371-2007>

1061

1062 Twomey, S. (1959). The nuclei of natural cloud formation part II: The supersaturation in natural
1063 clouds and the variation of cloud droplet concentration. *Geofisica pura e applicata*, 43(1),
1064 243–249. <https://doi.org/10.1007/BF01993560>

1065 Twomey, S. (1974). Pollution and the planetary albedo. *Atmospheric Environment* (1967), 8(12),
1066 1251–1256. [https://doi.org/10.1016/0004-6981\(74\)90004-3](https://doi.org/10.1016/0004-6981(74)90004-3)

1067 Veghte, D. P., Altaf, M. B., & Freedman, M. A. (2013). Size Dependence of the Structure of Organic
1068 Aerosol. *Journal of the American Chemical Society*, 135(43), 16046–16049.
1069 <https://doi.org/10.1021/ja408903g>

1070 Vepsäläinen, S., Calderón, S. M., & Prisle, N. L. (2023). Comparison of six approaches to predicting
1071 droplet activation of surface active aerosol – Part 2: Strong surfactants. *Atmos. Chem. Phys.*,
1072 23(23), 15149–15164. <https://doi.org/10.5194/acp-23-15149-2023>

1073 Vignes, A. (1966). Diffusion in Binary Solutions. Variation of Diffusion Coefficient with Composition.
1074 *Industrial & Engineering Chemistry Fundamentals*, 5(2), 189–199.
1075 <https://doi.org/10.1021/i160018a007>

1076 Virtanen, A., Joutsensaari, J., Koop, T., Kannosto, J., Yli-Pirilä, P., Leskinen, J., Mäkelä, J. M.,
1077 Holopainen, J. K., Pöschl, U., Kulmala, M., Worsnop, D. R., & Laaksonen, A. (2010). An
1078 amorphous solid state of biogenic secondary organic aerosol particles. *Nature*, 467(7317),
1079 824–827. <https://doi.org/10.1038/nature09455>

1080 Vitagliano, V., & Lyons, P. A. (1956). Diffusion Coefficients for Aqueous Solutions of Sodium Chloride
1081 and Barium Chloride. *Journal of the American Chemical Society*, 78(8), 1549–1552.
1082 <https://doi.org/10.1021/ja01589a011>

1083 Vizenor, A. E., & Asa-Awuku, A. A. (2018). Gas-phase kinetics modifies the CCN activity of a biogenic
1084 SOA [10.1039/C8CP00075A]. *Physical Chemistry Chemical Physics*, 20(9), 6591–6597.
1085 <https://doi.org/10.1039/C8CP00075A>

1086 Wallace, B. J., Price, C. L., Davies, J. F., & Preston, T. C. (2021). Multicomponent diffusion in
1087 atmospheric aerosol particles [10.1039/D0EA00008F]. *Environmental Science:
1088 Atmospheres*, 1(1), 45–55. <https://doi.org/10.1039/D0EA00008F>

1089 Wang, M., Wu, P., Sengupta, S. S., Chadhary, B. I., Cogen, J. M., & Li, B. (2011). Investigation of Water
1090 Diffusion in Low-Density Polyethylene by Attenuated Total Reflectance Fourier Transform
1091 Infrared Spectroscopy and Two-Dimensional Correlation Analysis. *Industrial & Engineering
1092 Chemistry Research*, 50(10), 6447–6454. <https://doi.org/10.1021/ie102221a>

1093 Werner, E. K., Hammond, M., & Bain, A. (2025). Surface tension predictions during hygroscopic
1094 growth and cloud droplet activation using a simple kinetic surfactant partitioning model.
1095 *Aerosol Science and Technology*, 59(7), 781–793.
1096 <https://doi.org/10.1080/02786826.2025.2465705>

1097 Wex, H., Stratmann, F., Topping, D., & McFiggans, G. (2008). The Kelvin versus the Raoult Term in the
1098 Köhler Equation. *Journal of the Atmospheric Sciences*, 65(12), 4004–4016.
1099 <https://doi.org/10.1175/2008JAS2720.1>

1100 Wiedensohler, A. (1988). An approximation of the bipolar charge distribution for particles in the
1101 submicron size range. *Journal of Aerosol Science*, 19, 387–389.

1102 Wolf, M. J., Zhang, Y., Zhou, J., Surratt, J. D., Turpin, B. J., & Cziczo, D. J. (2021). Enhanced Ice
1103 Nucleation of Simulated Sea Salt Particles with the Addition of Anthropogenic Per- and
1104 Polyfluoroalkyl Substances. *ACS Earth and Space Chemistry*, 5(8), 2074–2085.
1105 <https://doi.org/10.1021/acsearthspacechem.1c00138>

1106 Wu, L., Li, X., Kim, H., Geng, H., Godoi, R. H. M., Barbosa, C. G. G., Godoi, A. F. L., Yamamoto, C. I.,
1107 de Souza, R. A. F., Pöhlker, C., Andreae, M. O., & Ro, C. U. (2019). Single-particle
1108 characterization of aerosols collected at a remote site in the Amazonian rainforest and an
1109 urban site in Manaus, Brazil. *Atmos. Chem. Phys.*, 19(2), 1221–1240.
1110 <https://doi.org/10.5194/acp-19-1221-2019>

1111 Yang, F., Chen, H., Wang, X., Yang, X., Du, J., & Chen, J. (2009). Single particle mass spectrometry of
1112 oxalic acid in ambient aerosols in Shanghai: Mixing state and formation mechanism.

1113 *Atmospheric Environment*, 43(25), 3876–3882.
 1114 <https://doi.org/https://doi.org/10.1016/j.atmosenv.2009.05.002>

1115 Zhang, C., Lu, M., Ma, N., Yang, Y., Wang, Y., Größ, J., Fan, Z., Wang, M., & Wiedensohler, A. (2023).
 1116 Hygroscopicity of aerosol particles composed of surfactant SDS and its internal mixture with
 1117 ammonium sulfate at relative humidities up to 99.9%. *Atmospheric Environment*, 298,
 1118 119625. <https://doi.org/https://doi.org/10.1016/j.atmosenv.2023.119625>

1119 Zhang, Q., Jimenez, J. L., Canagaratna, M. R., Allan, J. D., Coe, H., Ulbrich, I., Alfarra, M. R., Takami,
 1120 A., Middlebrook, A. M., Sun, Y. L., Dzepina, K., Dunlea, E., Docherty, K., DeCarlo, P. F.,
 1121 Salcedo, D., Onasch, T., Jayne, J. T., Miyoshi, T., Shimon, A., . . . Worsnop, D. R. (2007).
 1122 Ubiquity and dominance of oxygenated species in organic aerosols in anthropogenically-
 1123 influenced Northern Hemisphere midlatitudes. *Geophysical Research Letters*, 34(13).
 1124 <https://doi.org/https://doi.org/10.1029/2007GL029979>

1125 Zhang, Y., Chen, Y., Lambe, A. T., Olson, N. E., Lei, Z., Craig, R. L., Zhang, Z., Gold, A., Onasch, T. B.,
 1126 Jayne, J. T., Worsnop, D. R., Gaston, C. J., Thornton, J. A., Vizuete, W., Ault, A. P., & Surratt, J.
 1127 D. (2018). Effect of the Aerosol-Phase State on Secondary Organic Aerosol Formation from
 1128 the Reactive Uptake of Isoprene-Derived Epoxydiols (IEPOX). *Environmental Science &*
 1129 *Technology Letters*, 5(3), 167–174. <https://doi.org/10.1021/acs.estlett.8b00044>

1130 Zhang, Y., Chen, Y., Lei, Z., Olson, N. E., Riva, M., Koss, A. R., Zhang, Z., Gold, A., Jayne, J. T.,
 1131 Worsnop, D. R., Onasch, T. B., Kroll, J. H., Turpin, B. J., Ault, A. P., & Surratt, J. D. (2019a).
 1132 Joint Impacts of Acidity and Viscosity on the Formation of Secondary Organic Aerosol from
 1133 Isoprene Epoxydiols (IEPOX) in Phase Separated Particles. *ACS Earth and Space Chemistry*,
 1134 3(12), 2646–2658. <https://doi.org/10.1021/acsearthspacechem.9b00209>

1135 Zhang, Y., Nichman, L., Spencer, P., Jung, J. I., Lee, A., Heffernan, B. K., Gold, A., Zhang, Z., Chen, Y.,
 1136 Canagaratna, M. R., Jayne, J. T., Worsnop, D. R., Onasch, T. B., Surratt, J. D., Chandler, D.,
 1137 Davidovits, P., & Kolb, C. E. (2019b). The Cooling Rate- and Volatility-Dependent Glass-
 1138 Forming Properties of Organic Aerosols Measured by Broadband Dielectric Spectroscopy.
 1139 *Environmental Science & Technology*, 53(21), 12366–12378.
 1140 <https://doi.org/10.1021/acs.est.9b03317>

1141 Zhang, Y., Sanchez, M. S., Douet, C., Wang, Y., Bateman, A. P., Gong, Z., Kuwata, M., Renbaum-
 1142 Wolff, L., Sato, B. B., Liu, P. F., Bertram, A. K., Geiger, F. M., & Martin, S. T. (2015). Changing
 1143 shapes and implied viscosities of suspended submicron particles. *Atmos. Chem. Phys.*,
 1144 15(14), 7819–7829. <https://doi.org/10.5194/acp-15-7819-2015>

1145 Zhu, J., Penner, J. E., Lin, G., Zhou, C., Xu, L., & Zhuang, B. (2017). Mechanism of SOA formation
 1146 determines magnitude of radiative effects. *Proceedings of the National Academy of*
 1147 *Sciences*, 114(48), 12685–12690. <https://doi.org/doi:10.1073/pnas.1712273114>

1148